

AD-A117 744

TECHNOLOGY SERVICE CORP SILVER SPRING MD  
ULTRALOW SIDELobe PLANAR NEAR FIELD MEASUREMENT STUDY.(U)  
JUN 82 K R GRIMM

F/6 20/14

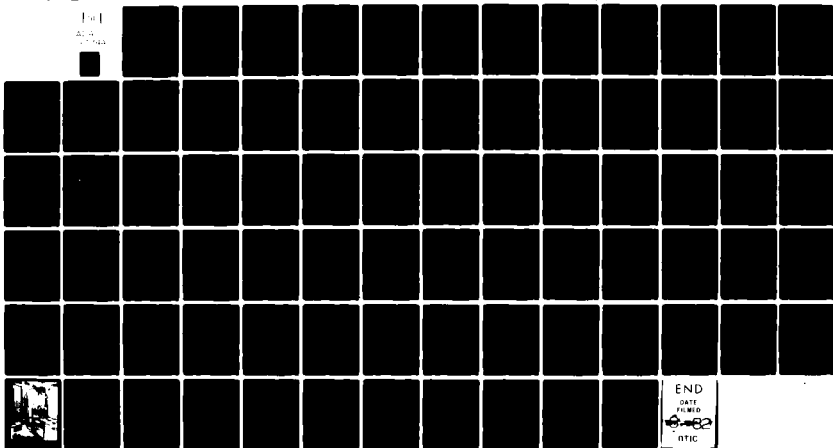
UNCLASSIFIED

TSC-W41-142/RAD

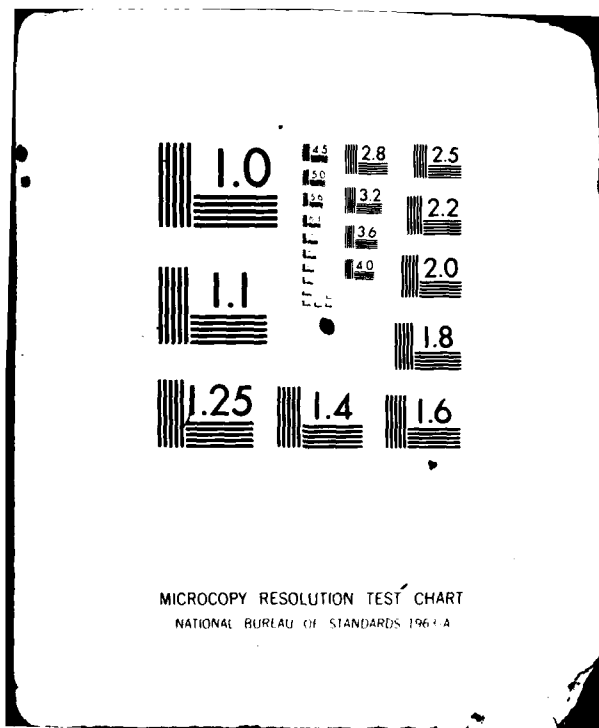
N00014-82-C-0115

NL

FILE  
AD-A117 744



END  
DATE  
FILMED  
82  
NTIC



12

# Technology Service Corporation

Washington Operations: 8555 Sixteenth Street, Silver Spring, Maryland 20910 Phone: (301) 565-1970

Ref: TSC-W41-142/rad  
B7431111

AD A 11 7744

## FINAL REPORT

### ULTRALOW SIDELOBE PLANAR NEAR FIELD MEASUREMENT STUDY

K. R. Grimm

Technology Service Corporation  
8555 16th Street  
Silver Spring, Maryland 20910

30 June 1982

Final Report for Period 1 January 1982 - 30 June 1982

Approved for Public Release;  
Distribution Unlimited

Prepared for:

Office of Naval Research  
800 N. Quincy Street  
Arlington, Virginia 22217

Naval Sea Systems Command  
Code 62R13  
Washington, D. C. 20362

DTIC  
ELECTE  
JUL 30 1982

E

DTIC FILE COPY

82 07 30 082

UNCLASSIFIED

SECURITY CLASSIFICATION OF THIS PAGE (When Data Entered)

REPORT DOCUMENTATION PAGE		READ INSTRUCTIONS BEFORE COMPLETING FORM
1. REPORT NUMBER TSC-W41-142/rad	2. GOVT ACCESSION NO. AD-A117744	3. RECIPIENT'S CATALOG NUMBER
4. TITLE (and Subtitle) Ultralow Sidelobe Planar Near Field Measurement Study		5. TYPE OF REPORT & PERIOD COVERED Final Report 1 Jan 1982-30 June 1982
		6. PERFORMING ORG. REPORT NUMBER
7. AUTHOR(s) K.R. Grimm		8. CONTRACT OR GRANT NUMBER(s) N00014-82-C-0115
9. PERFORMING ORGANIZATION NAME AND ADDRESS Technology Service Corporation 8555 16th Street, Suite 300 Silver Spring, Maryland 20910		10. PROGRAM ELEMENT, PROJECT, TASK AREA & WORK UNIT NUMBERS B74311
11. CONTROLLING OFFICE NAME AND ADDRESS Office of Naval Research (614A) 800 N. Quincy Street Arlington, Virginia 22217		12. REPORT DATE 30 June 1982
		13. NUMBER OF PAGES 74
14. MONITORING AGENCY NAME & ADDRESS (if different from Controlling Office) Naval Sea Systems Command (62R13) Washington, D.C. 20362		15. SECURITY CLASS. (of this report) UNCLASSIFIED
		15a. DECLASSIFICATION/DOWNGRADING SCHEDULE
16. DISTRIBUTION STATEMENT (of this Report)  Approved for Public Release; Unlimited Distribution		
17. DISTRIBUTION STATEMENT (of the abstract entered in Block 20, if different from Report)		
18. SUPPLEMENTARY NOTES  Prepared under the Defense Small Business Advanced Technology (DESAT) Program - Phase 1.		
19. KEY WORDS (Continue on reverse side if necessary and identify by block number) Array Antenna Near Field Testing Error Analysis		
20. ABSTRACT (Continue on reverse side if necessary and identify by block number) An analytic study has extended existing methods of estimating antenna pattern errors when testing by the method of planar near field probing. Improved error bounds are given for very low sidelobe levels based only on the measured near field data and known tolerances due to probe positioning and multipath. These bounds are useful for certifying array performance independent of standard far field antenna range tests. They also can serve as improved design criteria for the construction of quality near field		

DD FORM 1473 EDITION OF 1 NOV 65 IS OBSOLETE

UNCLASSIFIED

SECURITY CLASSIFICATION OF THIS PAGE (When Data Entered)

UNCLASSIFIED

SECURITY CLASSIFICATION OF THIS PAGE(When Data Entered)

Testing systems. An optimum probe for low sidelobe testing is shown to be one which minimizes its back scatter while simultaneously contributing minimum mean square error to the sidelobe region. That this is impossible for the commonly used dominant-mode waveguide probes is shown, and a recommendation is made to design an alternate probe based on a single (or small array cluster) of radial mode dipoles. Finally, the feasibility of a highly thinned measurement/processing technique is shown using existing Navy owned near field data from a moderate sidelobe array. The principle study recommendation is to confirm the improved error estimates developed herein by conducting a test of a qualified very low sidelobe array at the National Bureau of Standards, in order to demonstrate the fundamental limits of measurement accuracy of planar near field probing.

UNCLASSIFIED

SECURITY CLASSIFICATION OF THIS PAGE(When Data Entered)

## PREFACE

This study is based on the original work of A. D. Yaghjian and A. C. Newell at the National Bureau of Standards (NBS) and E. B. Joy and G. K. Huddleston at Georgia Institute of Technology, whose combined efforts with both experimental and analytic Planar Near Field (PNF) theory is largely responsible for the wide acceptance of this relatively new antenna measurement method. The first successful PNF test with an electronic array was performed at NBS in 1973, and major goal of the present program is to replicate those original tests using a qualified very low sidelobe array.

During this initial study, several new probing techniques have been examined which can improve existing sidelobe measurement accuracy. These include probe-position error compensation schemes and optimum probes for low sidelobe pattern testing. In addition, the method of estimating the effects of near field multipath has been extended. It is shown that existing sidelobe error models should be scaled to reflect the multipath phase error unique to each test antenna and probe scanner. A plan for conducting a very low sidelobe testing demonstration is outlined in the appendix, and is recommended as a phase 2 continuation of this present Defense Small Business Advanced Technology (DESAT) investigation.



Accession For	
NTIS GRA&I	<input checked="checked" type="checkbox"/>
DTIC TAB	<input type="checkbox"/>
Unannounced	<input type="checkbox"/>
Justification	
By	
Distribution/	
Availability Codes	
Dist	Avail and/or Special
A	

## TABLE OF CONTENTS

1.0	INTRODUCTION .....	1
1.1	General .....	1
1.2	Background .....	1
1.3	Previous Studies .....	2
1.4	Present Investigation .....	2
2.0	PROBLEM FORMULATION .....	3
2.1	Sources of Error .....	3
2.2	Fractional Error Ratio .....	3
3.0	IMPROVED BOUNDS ON FUNDAMENTAL MEASUREMENT ERRORS ....	13
3.1	Probe Position-Error Compensation .....	13
3.2	Multipath Effects .....	20
4.0	IMPROVED SAMPLING CONCEPTS .....	31
4.1	Reduced Scattering Probe .....	31
4.2	Minimum Sampling Schemes .....	34
4.3	Optimum Probes .....	41
5.0	CONCLUSIONS AND RECOMMENDATIONS .....	52
5.1	General .....	52
5.2	Principal Conclusions .....	52
5.3	Results .....	53
5.4	Recommendation .....	55
6.0	REFERENCES .....	56
APPENDIX A - Preliminary Test Plan for the Ultralow Sidelobe Near Field Measurement Study for DESAT Phase 2 Demonstration .....		58

## 1.0 INTRODUCTION

### 1.1 General

Planar Near Field (PNF) antenna scanning has come into increasing use for the testing of microwave array antennas which have been designed for use in advanced DOD electronic systems. This measurement technique is attractive because it is based on short-range distances, is easily accommodated indoors, and because it is inherently accurate, since so few measurement approximations are involved. It does however, require the acquisition of large sets of PNF data, and the execution of a computer data transform in order to recover the desired test antenna's Far Field (FF) properties. The purpose of this study is to estimate the accuracy by which this may be accomplished for an arbitrary low sidelobe array.

### 1.2 Background

Many previous PNF testing programs have been conducted in specific applications. These include tests of X-band lens arrays and electronically steerable arrays [1], large wideband reflectors [2], precision feeds for very large reflectors [3], on-aircraft antennas [4], and even broadbeam horns [5]. Probably the best known PNF test programs are those now underway for the production testing of radar arrays used in the US ARMY TPQ-36/37 Projectile Locator System, and in the US Navy AEGIS AN/SPY-1A Shipboard Missile System. In all of these testing exercises, the question of measurement accuracy has been resolved by comparing the NF result to a standard figure-of-merit, i.e., to an antenna pattern measured on a qualified FF range. However, with increasingly stiffer performance requirements being demanded from the array, trustworthy FF "standard patterns" are indeed difficult (and expensive) to acquire. Consequently bounding expressions for FF error based only on NF parameters are necessary for independent accuracy estimation, as well as for specifying criteria useful for the original design of the NF facility.



### 1.3 Previous Studies

Several earlier measurement analyses have been completed, both to demonstrate the accuracy of the PNF method, and to provide guidance for facility design. Rodrigue, Joy, and Burns introduced simulated measurement error into theoretical NF distributions, and then computed the resulting FF parameter errors [6]. Newell performed a similar analysis, but used measured NF data (assumed error free) acquired during the first PNF test of an electronic phased array during a 1973 technology study at NBS [7]. Then in 1976 Yaghjian completed an independent analysis for estimating possible FF pattern error for the PNF test of an arbitrary microwave antenna [8]. Together, these last two papers are considered the basic references for error-prediction in any PNF application.

### 1.4 Present Investigation

The present effort seeks to expand upon the NBS analyses by re-evaluating selected error expressions for their applicability in low sidelobe testing problems. "Low Sidelobe" refers to relative field levels which may be radiated in any of the antennas modes, pattern planes, or polarizations which are at least 30dB below the antenna's peak directivity. The approach of this study is to apply, and modify as necessary, existing error bounds when applied to an arbitrary low sidelobe array. Study goals have included:

- prioritize real PNF measurement error sources
- modify existing facility design criteria
- point toward possible new PNF probing techniques, and
- establish fundamental measurement accuracy limits.

In this approach only the planar scanning geometry is considered, although cylindrical and spherical geometries have also been in use [9].

A secondary goal is to exercise an alternate (i.e., not FFT-based) processing algorithm, using actual Navy-owned PNF test data. The algorithm called "Collapse," allows thinning of the normal two-dimensional NF sampling grid, and has the potential for simplifying both scanner design and processing techniques in future low sidelobe PNF testing applications.

## 2.0 PROBLEM FORMULATION

### 2.1 Sources of Error

A general test array is assumed to be operating in free space, in a single mode and frequency such that the desired radiation is directed normally outward through its mechanical or electronically steered pointing direction. A planar NF probing scanner is situated close to (and nearly parallel to) the array aperture. (see sketch in Figure 1). For this type of test, possible FF pattern errors will be due to NF measurement errors, including

- sampling area truncation
- probe positioning errors
- RF instrument conversion errors
- multiple probe/array reflections
- probe pattern and numerical transform uncertainties

### 2.2 Fractional Error Ratio

If  $E(r)$  is the electric field in the direction  $r$  to within the limits of error, and  $\pm \Delta E(r)$  is the limit of error involved with measuring  $E(r)$ , then a fractional error ratio may be written as

$$\eta(r) = \left| \frac{|E(r) \pm \Delta E(r)| - |E(r)|}{|E(r)|} \right| \leq \frac{|\Delta E(r)|}{|E(r)|} \quad (1)$$

From this ratio, the FF dB gain error is easily found,

$$\eta^{dB} = 20 \log(1 + \eta(r)) \quad (2)$$

The following subsections summarize existing methods for computing  $\eta(r)$  for selected NF error sources and at arbitrary low sidelobe pattern levels. Then in later sections, these sources are analyzed to suggest possible improved NF probing techniques capable of compensating the principle NF measurement errors.

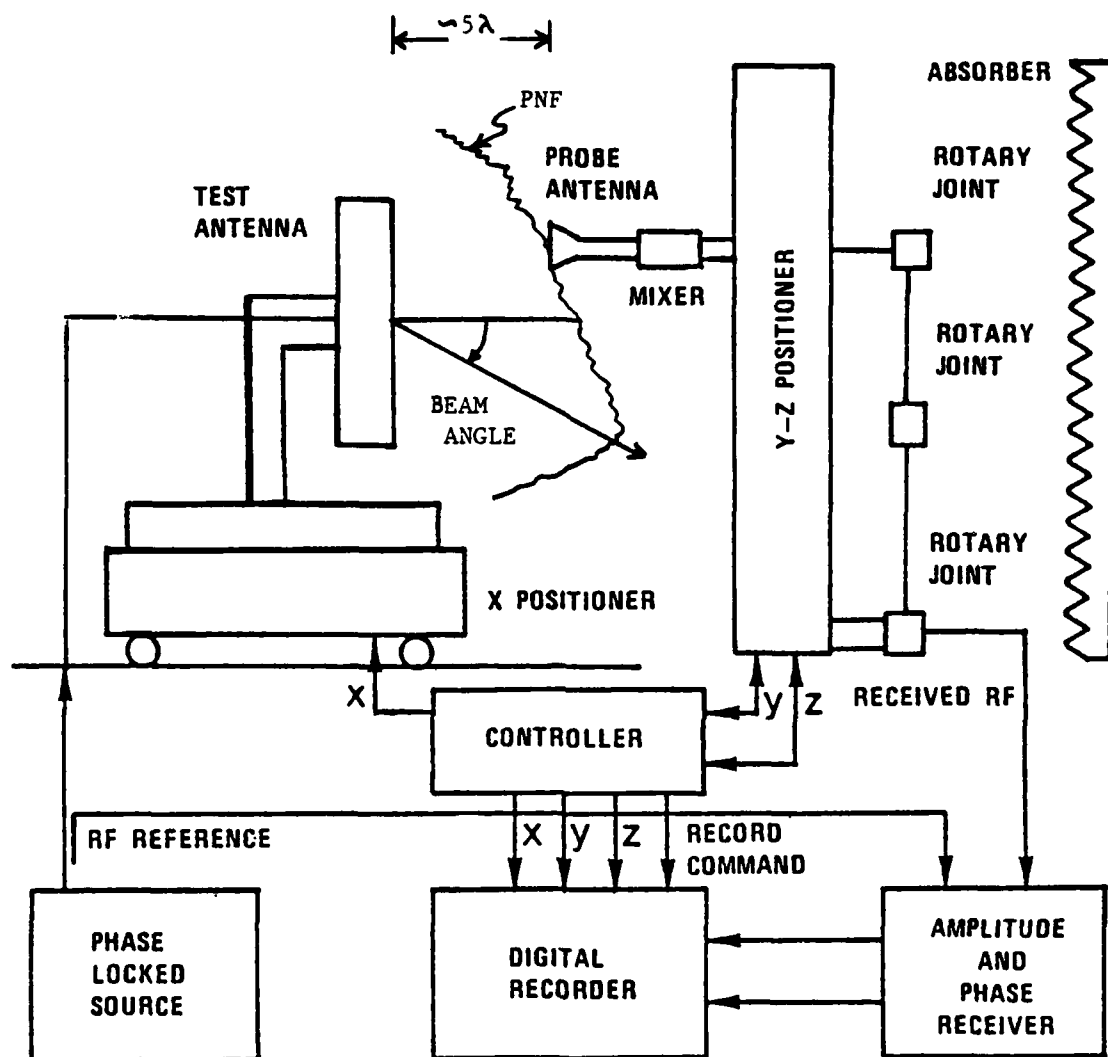


Figure 1. Basic Planar Near Field (PNF) Measurement

### 2.2.1 Scan Length Truncation

Far Field sidelobe error contributed by finite scan area limitations depend primarily upon the value of the edge fields at the limit of scan, the design illumination, the RF wavelength, and the probe separation distance. Outside the solid angle  $\theta_c$  in Figure 2, no accurate FF sidelobes may be transformed from NF data acquired on a scanner whose geometry is as shown. When physical scan length limitations are not severe, this measurement error source does not fundamentally limit sidelobe measurement accuracy. Of course, the selection of the minimum required scan length is a principle NF facility design parameter, and is also closely related to the optimum probe pattern (section 4.3). Within the  $\theta_c$ , the worst case FF fractional error at the error-free pattern level  $g(r)$ , for center line scanning is:

$$\eta(r) \leq \frac{\alpha \lambda L^{\max} 10^{-X/20}}{2 A \sin \theta_{\max}} g(r) \quad (3)$$

where

$\alpha$  = NF taper factor

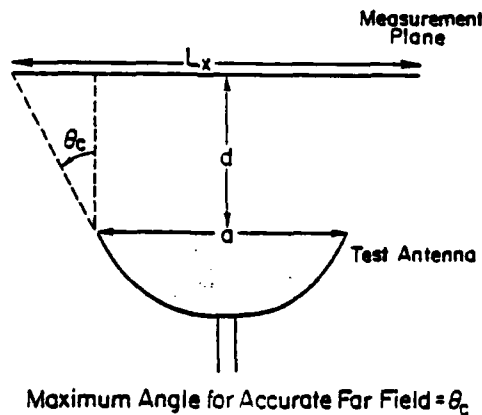
$\lambda$  = RF wavelength

$L^{\max}$  = line scan maximum length

$A$  = test array area

$X$  = edge NF value (dB)

$g(r)$  = error-free pattern level of interest (numeric)



$$\theta_c \approx \tan^{-1} \left( \frac{L_x - a}{2d} \right)$$

Figure 2. Scan Length Truncation Geometry

## 2.2.2 Probe XY-Position Errors

The basic error analysis of Newell [7] has already determined the form of the worst case probe transverse (XY) position error. "Worst-case" is defined to mean capable of generating the peak possible sidelobe error, i.e., a realizable peak error. (Probable error is discussed in section 3.1.) His approach used the Schwartz inequality and the Fourier Transform to establish position error bounds. For a single "cut" NF measurement having the assumed form, with X-scan  $B(x) = a(x)e^{i\phi(x)}$ , the realizable worst case X-position error will have the form

$$\text{Nonsteered Beam: } \Delta(x) = ca'(x) \cos(k_3 x) \quad (4a)$$

$$\text{Steered Beam: } \Delta x = c a(x) k_b \cos((k_b - k_3)x) \quad (4b)$$

where prime indicates derivative by x, and

$k_3$  is the sidelobe angle

$k_b$  is the beam steering angle

c is a complex normalizing constant based on the RMS of the scanner's actual position error distribution.

Newell concludes that this worst case probe position error will be systematic (structured), and will have a low frequency periodicity. This type of error is quite realizable, even in carefully-designed scanners. Based on this analysis, several simple bounding estimates for sidelobe error have been in use by PNF facility designers. These bounds predict possible FF sidelobe error in terms of NF parameters only, and are given as

$$\text{Nonsteered Beam: } \eta_{dB} \leq 4.3 \frac{D(0)}{D(k_a)} \frac{\Delta_{x,y}}{L} \quad (5a)$$

$$\text{Steered Beam: } \eta_{dB} \leq 13.5 \left( \frac{D(k_b)}{D(k_a)} \right) \frac{\Delta_{x,y}}{\lambda} \sin \theta_b \quad (5b)$$

where

$D(0)/D(k_a)$  is the pattern level at angle  $k_a$

$D(k_b)/D(k_a)$  is the pattern level at angle  $k_a$  when steered to  $k_b$

L is the array maximum linear dimension

$\theta_b$  is the polar steering angle.

In general, periodic XY probe positioning error will lead to FF paired-error lobes which are quite large, but only for steered beam testing. Insignificant sidelobe errors result for nonsteered beams. (The principle effect is on beam gain). To show how steered beam error lobes are erroneously generated by a periodic X-position error and predicted by equation (5b), Newell has performed a simulation which introduced artificial NF error proportional to the worst-case position error into actual PNF data (assumed error free). The artificial error had a peak deflection of  $.1\lambda$  and a periodicity given by equation (4b). The pattern produced from the error-free PNF data is reproduced here as the solid line in Figure 3, whereas the dotted curve is the same pattern from the corrupted NF. The top curve plots the difference between the two patterns in percent of peak. The simulation indicates that steered beam PNF testing with a scanner having a worst-case position error with peak deflection of  $.1\lambda$ , will generate near-in sidelobe errors of nearly 20 dB at the -35 dB level. Such a scanner is obviously unacceptable for low sidelobe testing. A suggested improved probing technique which minimizes the effect of these possible XY probing tolerances is given in Section 3.1.4, along with an analysis which is useful for estimating the expected sidelobe error with specified confidence.

### 2.2.3 Probe Z-Position Errors

Sidelobe errors due to scanner Z-tolerances are estimated in a manner nearly identical to the procedure used for predicting XY probe position errors on steered beam patterns. Although probe error due to either scanner rotation or constant offset do not contribute to sidelobe error, periodic Z-position error in the measured NF is responsible for significant sidelobe error in both the steered and nonsteered beam patterns. The worst-case Z-position error has been shown to have the form:

$$\text{All Beams: } \Delta z(x) = \Delta_z a(x) \sin(\phi(x) - \frac{2\pi}{\lambda} x \sin \theta_b) \quad (6)$$

when the measured NF is assumed to be  $B(x, z') = a(x, z') e^{i\phi(x, z')}$  with  $z' = d + \Delta z(x)$  and the beam is steered to  $\theta_b$ .  $\Delta_z$  is the peak Z-displacement error.

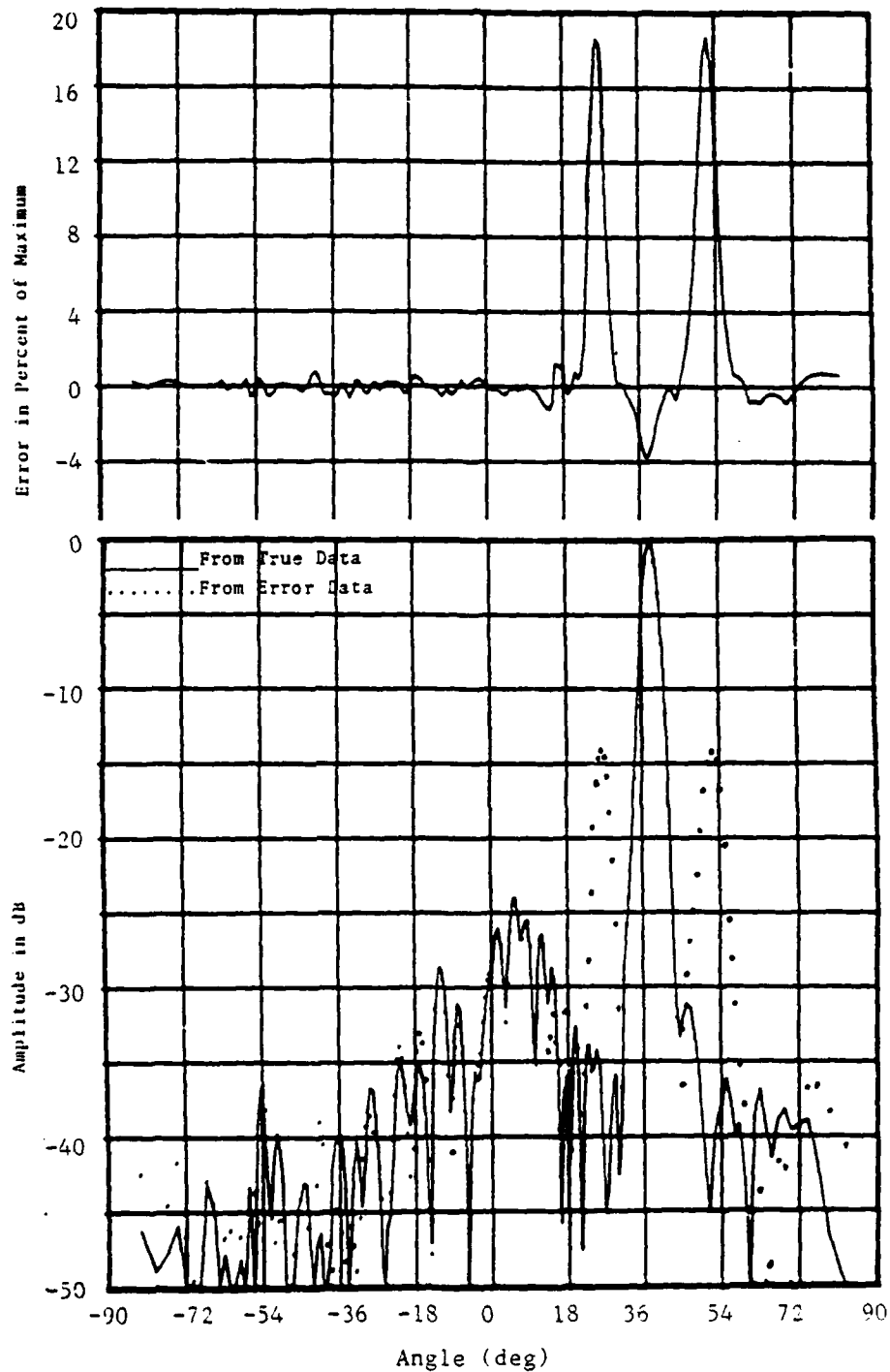


Figure 3. Sidelobe Error from Actual PNF Data Corrupted by Simulated Worst-Case X-Position Error of  $\Delta_x = .1\lambda$  [Newell Ref. 7]

The form of this worst-case Z-error is proportional to the NF amplitude modulated by a periodic function which depends upon the Z-displacement and the specified FF sidelobe direction (and mainbeam pointing for steered beams). Then, the FF error bounds are:

$$\begin{array}{l} \text{Nonsteered:} \\ \text{Beam} \end{array} \quad \eta_{\text{dB}} \leq 13.5 \left| \frac{D(0)}{D(k_a)} \right| \left( \frac{\Delta Z}{\lambda} \right) \quad (7a)$$

$$\begin{array}{l} \text{Steered:} \\ \text{Beam} \end{array} \quad \eta_{\text{dB}} \leq 13.5 \left| \frac{D(k_b)}{D(k_a)} \right| \left( \frac{\Delta Z}{\lambda} \cos \theta_b \right) \quad (7b)$$

where the terms have been defined following equation (6).

#### 2.2.4 Instrumentation Error

Receiver inaccuracies when measuring NF phase corrupt the transformed sidelobes with the same functional form as do probe Z-positioning errors. Since instrumentation phase error usually increases with decreasing NF amplitude, this measurement uncertainty will produce no serious error in the FF sidelobes. If however, the instrumentation phase error is periodic, or otherwise structured in the NF regions of relatively high amplitude, then sidelobe errors are likely. Worst case sidelobe error due to RF instrumentation phase error is given as:

$$\eta(r) \leq \Delta\phi_{\text{max}} g(r)/2 \quad (8)$$

where

$\Delta\phi_{\text{max}}$  is the radian phase measurement error within the NF region  
where the amplitude is  $> -15$  dB relative to peak

$g(r)$  is pattern level of interest

Unlike most forms of instrumentation phase error, instrumentation amplitude error is a primary source of sidelobe error. In the near-in sidelobe region, this error is contributed primarily by the dB/dB inaccuracy of the test RF link, and the NF taper factor  $\alpha$ . Instrumentation amplitude error increases with the decreasing design sidelobe level, but is nearly



zero for the highest sidelobes (uniform illumination). The worst case sidelobe error bound, due to instrumentation amplitude error is:

$$\eta(r) \leq 2 N_{dB} \beta \quad (9)$$

where

$N_{dB}$  is the relative amplitude inaccuracy from all sources in the test channel expressed in dB error per dB amplitude from peak

$$\beta = \begin{cases} \alpha - 1 & \dots \text{Near-in sidelobes} \\ \frac{\alpha \lambda L_{\max}}{3} & \dots \text{Far-out sidelobes} \end{cases}$$

#### 2.2.5 Multipath Error

Multiple reflections between probe and array, and between probe and chamber generate interference patterns in the measured NF, which if small enough are usually neglected during the test. However, the existing bound on the predicted sidelobe error is rather large, and not in agreement with practical measurement experience. A principle topic of this study is the reconsideration of this multipath bound in section 3.2.

Nevertheless, the existing upperbound multipath error ratio is estimated from:

$$\eta(r) \leq \epsilon^{mr} g(r) \quad (10)$$

where

$\epsilon^{mr}$  is a measured peak interference magnitude  
 $g(r)$  is the specified sidelobe level of interest

#### 2.2.6 Composite Sidelobe Error Summary

A relative comparison of the effects on sidelobes due to each of the NF error sources, as summarized in this section, is shown in Figure 4. These curves plot the predicted upperbound sidelobe error for a nonsteered  $\Sigma$  mode pattern whose assumed properties (and also that of the testing facility) are given in Table 1.

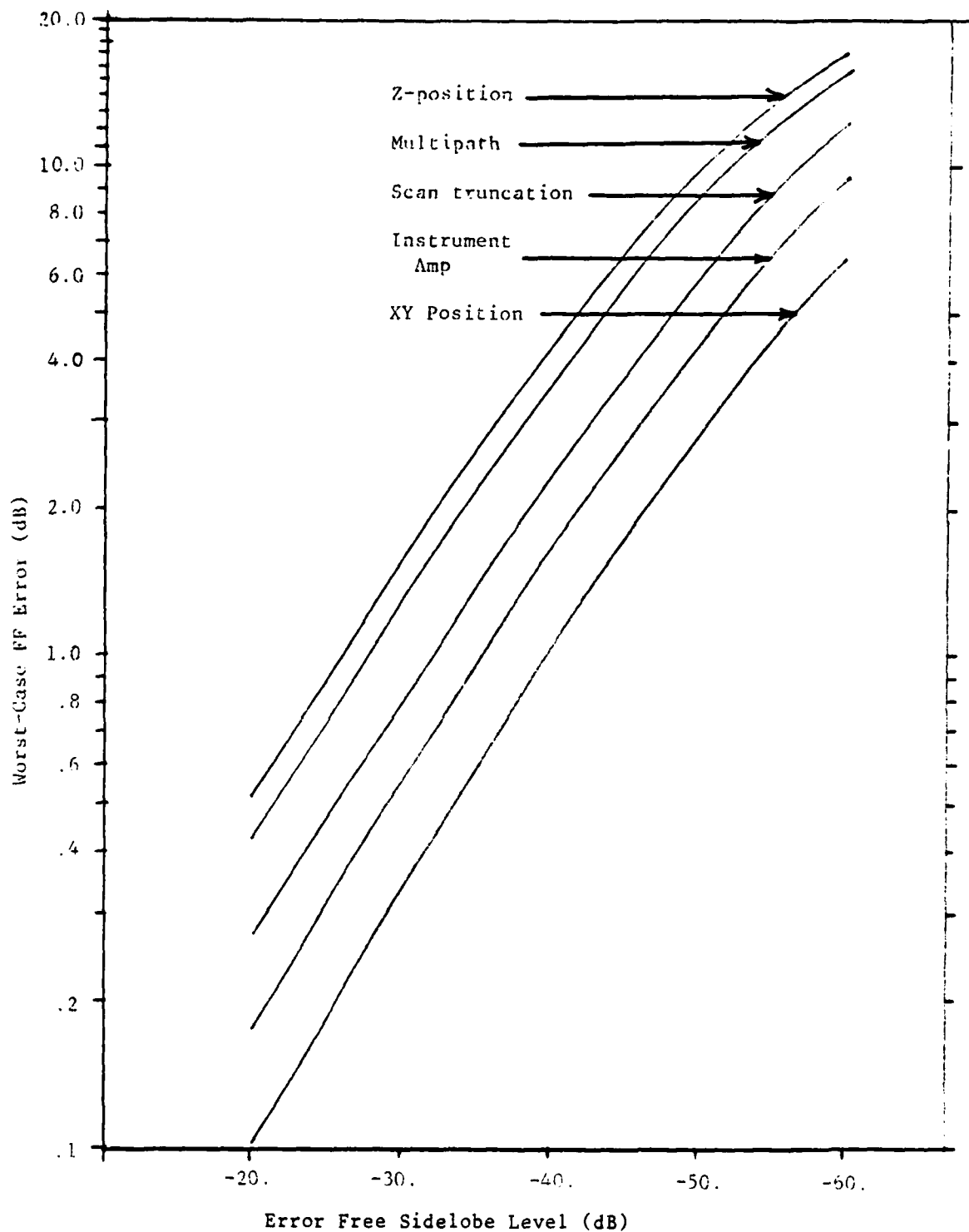
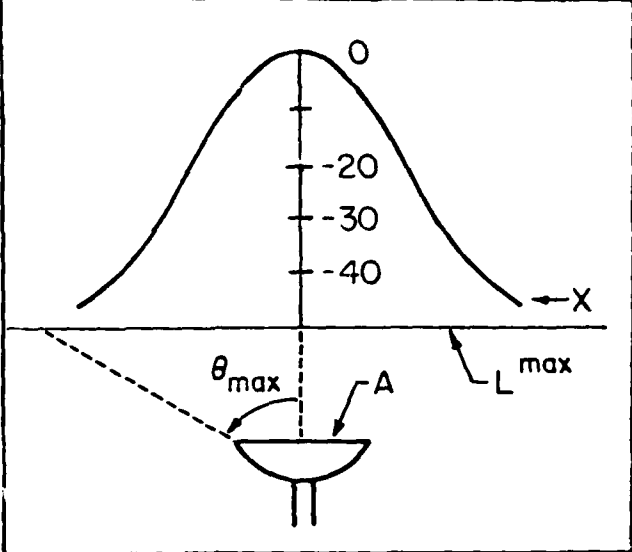


Figure 4. Upperbound FF Sidelobe Error for the Assumed Array and Facility in Table 1 using the Existing Error Model of Newell and Yaghjian [Ref. 7,8].

Table 1. Properties of Assumed Array and PNF Facility  
for Estimating Upperbound Sidelobe Errors

	Parameter	Value
	NF taper factor ( $\alpha$ )	3
	RF wavelength ( $\lambda$ )	3.26 cm
	Maximum Scan length ( $L^{\max}$ )	160 cm
	Test Antenna Area (A)	5000 cm <sup>2</sup>
	FF cutoff angle ( $\theta_c$ )	60°
	Edge NF magnitude (X)	-45 dB
	Instrumentation Amp Error ( $N_{dB}$ )	.01 dB/dB
	Maximum antenna dimension ( $l^{\max}$ )	80 cm
	Peak X-position error ( $\Delta X$ )	.2 mm
	Peak Z-position error ( $\Delta Z$ )	.2 mm
	Multipath ratio ( $\epsilon^{mr}$ )	.01

These curves show the expected worst-case error at various sidelobe levels for each of the possible NF measurement error sources. Clearly, the Z-position error and multiple error are most degrading, for the reasonable assumptions made in Table 1, which were selected to represent the performance of the NBS PNF scanner of the time of its completion (1975). Only the relative differences among the curves in Figure 4 support the "most-degrading" statement above, but absolute sidelobe error for each source is upperbound, i.e., least probable. The more probable sidelobe errors are the basis of what follows.

### 3.0 IMPROVED BOUNDS ON FUNDAMENTAL MEASUREMENT ERRORS

From the example of the last section, accurate low sidelobe pattern testing by PNF probing finally depends upon minimizing both probe position error and the multiple reflection between probe and array. In typical applications, these two sources of error alone dominate all contributors in the measurement process, and their possible compensation are considered in this section. Additional improved sampling techniques are described in section 4. The most promising of these are proposed for demonstration during the DESAT Phase 2 investigation.

#### 3.1 Probe Position-Error Compensation

To reduce the magnitude of sidelobe error due to imperfect probe positioning, a method to compensate the measured NF data before transform has been suggested [10]. In this scheme, actual probe deviations from the desired planar sampling grid are measured everywhere in the scan plane, and then used to modify NF data as if it had been acquired on a true planar surface. The complete compensation is for both amplitude and phase and for every propagation angle at each measurement point. However, the additional processing load that this complete compensation implies, is burdensome even with present computers. Consequently, a modified compensation has been developed. Called "K-space correction," this technique adds a phase-only increment to the measured NF, which is proportional to the beam pointing direction and to the pre-measured vector position error at each sample point [11]. The precise probe location data required for this compensation can be found using LASER optical distance measuring instruments. That phase-only position error correction is a useful scheme for compensating a fundamental PNF measurement error source is shown next. The form of the residual error (following compensation) is described in Section 3.1.3.

##### 3.1.1 Utility of Phase-only Compensation

The error-free general one dimensional NF is again assumed to be of form  $B(x, z) = a(x, z)e^{i\phi(x, z)}$ , and its change due to Z-error only,\*

---

\* a similar analysis can be given for XY position error

is written by a partial Taylor expansion as

$$B(x, z') = B(x, z) + \frac{\partial B(x, z)}{\partial z} \Delta z(x) \quad (11)$$

By invoking the Fourier relation between  $B(x, z)$  and its spectrum  $D(k_x)$ , the derivative in (11) becomes,

$$\frac{\partial B(x, z)}{\partial z} = iC\gamma(k_x) \underbrace{\int D(k_x) e^{i\gamma z} e^{ik_x x} dk_x}_{B(x, z)} \quad (12)$$

where  $C$  is a constant and  $\gamma(k_x)$  is the Z-directed propagation constant given by  $\sqrt{(\frac{2\pi}{\lambda})^2 - k_x^2}$  for real space.

The partial derivative may also be written directly from the general linear NF as:

$$\begin{aligned} \frac{\partial B(x, z)}{\partial z} &= \frac{\partial}{\partial z} \{ a(x, z) e^{i\phi(x, z)} \} \\ &= a'(x, z) e^{i\phi(x, z)} + i\phi'(x, z) B(x, z) \end{aligned} \quad (13)$$

Equating (12) and (13), find

$$a'(x, z) e^{i\phi(x, z)} + i\phi'(x, z) B(x, z) = i\gamma(k_x) B(x, z) \quad (14)$$

From this last equation, it is concluded that:

$$\begin{aligned} a'(x, z) &\approx 0 \\ \phi'(x, z) &\approx \gamma(k_x) = \frac{2\pi}{\lambda} \cos\theta_{\text{steering}} \end{aligned} \quad (15)$$

which states that due to Z-position error only, the NF amplitude change is negligible, but the NF phase change is large. Thus, the fundamental measurement accuracy imposed by the positioning error of the "as-built" scanner, can be extended by a pre-processing routine which adds a synthetic phase increment to the measured NF data prior to performing the transform. This procedure removes from the data, the effects of real systematic probe position error. What remains is a data set whose residual position errors are random only across the scan plane, as sketched in Figure 5. The sketch shows possible

single scan NF position error before and after compensation. The relative large random deflections in the top sketch are superimposed over an even larger systematic error whose worst-case form was given in equations (4, 6). The process of LASER corrections accurately finds the error  $\Delta_p$  at each sample point, and compensates the NF data accordingly. The center trace gives the residual, i.e., compensated position error, now entirely random, whose statistics we seek to estimate in order to compute sidelobe error.

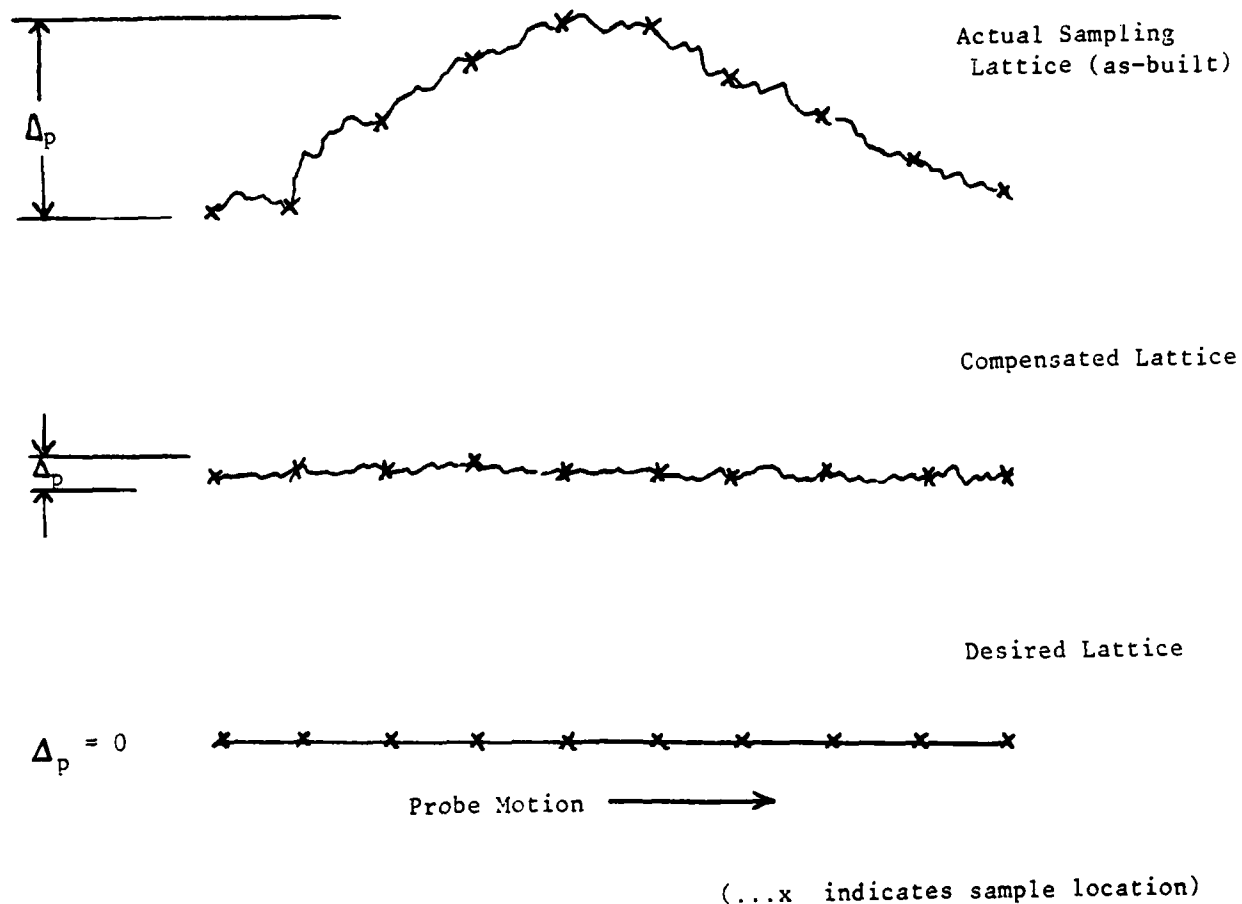


Figure 5. Sketch of NF Probe Positions Along a Single Scan Showing the Effect of Phase-only Position Error Compensation

### 3.1.2 Random Position Error

If a scanner is so precisely built (or position-error compensated as just described), then due only to random positioning error, a reduced sidelobe error bound may be found. This new bound will give probable sidelobe errors, rather than worst-case or upperbound errors. The probable error will be estimated by the same equation as previously used (e.g., (7) for Z-position error), but now the probable value of a particular position error will be specified from a random position error density. (Essentially, this is the same approach used by Allen to estimate sidelobe level probabilities based on the values of illumination error occurring randomly among the array elements [12]). The variance and the peak value of the compensated position errors will depend upon the actual as-built positioning imprecision, and the exact manner of compensation. The essential point, however, is that worst-case systematic positioning error is eliminated by phase-only correction, leaving only residual error deviation to contribute to sidelobe error. Probable sidelobe error, then, is estimated from (5, 7) by selecting a value of residual error whose probability of occurrence can be specified. Only a knowledge of the residual position error density is needed to make these estimates.

### 3.1.3 Residual Position Error Density

The process of using LASER optics to measure actual probe locations is so precise that peak position errors can be found with nearly absolute confidence. Within these measured peaks, however, it can be assumed that the magnitude of any other lesser error is approximately gaussian distributed.\* Thus the probability density for the residual position error may be considered to be a truncated normal random variable as sketched in Figure 6. The mean error  $U_0$ , and the peak random error  $X_0$  are indicated in the sketch. Only the mean deviation,  $\sigma_n$ , is important since constant offset (or mean) error does not contribute to sidelobe error. The standard deviation of the residual position error depends upon the measured peak error as next described.

---

\* We make this assumption only to find closed-form expressions for bounding the residual error, but in actual practice, one can measure position errors everywhere in the scan plane, and construct the unique error density for those data.

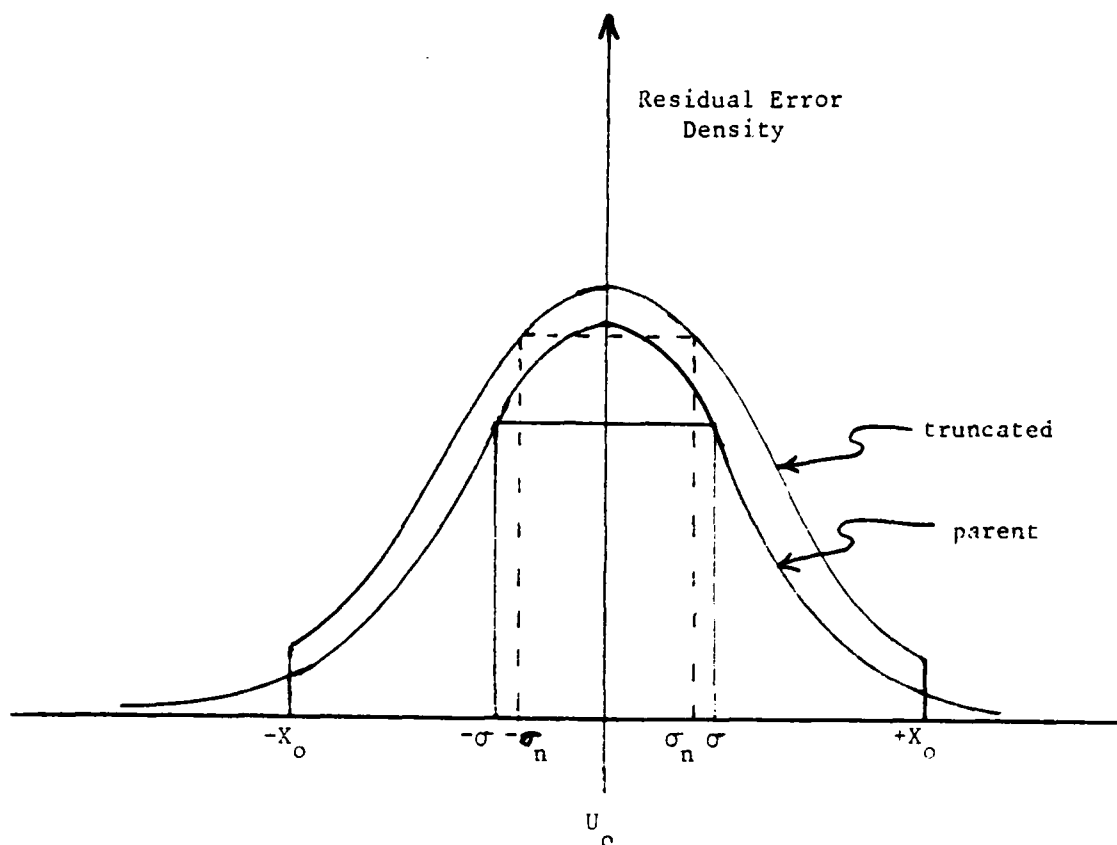


Figure 6. Sketch of Truncated Gaussian Error Density to Model Residual Position Error Following Phase-only Compensation

#### 3.1.4 Variance of Truncated Error Density

The residual error is a truncated gaussian random variable whose density is normalized by the excluded probability of having a position error larger than the peak error, i.e., the density (for a zero-mean process) is

$$f_1(x) = \begin{cases} \frac{1}{F(X_o) - F(-X_o)} \frac{e^{-x^2/2\sigma^2}}{\sqrt{2\pi\sigma^2}} & |x| \leq X_o \\ 0 & |x| > X_o \end{cases} \quad (16)$$



where  $F$  is the probability of the standard gaussian density, and  $\sigma^2$  is its variance. The desired variance,  $\sigma_n^2$ , in terms of parent parameters is:

$$\text{var}(X_o) = \frac{1}{F(X_o) - F(-X_o)} \int_{-X_o}^{X_o} \frac{x^2 e^{-x^2/2\sigma^2}}{\sqrt{2\pi\sigma^2}} dx$$

which, by change of variables, integrates straightforwardly to be:

$$\sigma_n^2 = \sigma^2 \left[ \left( \frac{1 - 2X_o}{\sqrt{2\pi\sigma^2}} e^{-X_o^2/2\sigma^2} \right) \left( \frac{1}{F(X_o) - F(-X_o)} \right) \right]$$

And for  $\sigma^2 = 1$  in the parent density,  $\sigma_n^2$  of the residual-error density simplifies to:

$$\sigma_n^2 = \frac{1 - \sqrt{2/\pi} X_o e^{-X_o^2/2}}{F(X_o) - F(-X_o)} \quad X_o \geq 0 \quad (17)$$

which is plotted in Figure 7 for a range of possible peak error  $X_o$  in units of  $\sigma$ . The plot shows that the residual position error density always has a smaller standard deviation than does the parent distribution, but approaches a true gaussian curve for large peak errors. Thus, if the actual peak scanner errors were originally only 50% larger than the observed  $1.0\sigma$  deviation of all position errors ( $X_o = 1.5\sigma$  in Figure 7), then the compensated deviation is reduced by 27% ( $\sigma_n^2 = .73\sigma^2$ ). The analysis also predicts a 35% reduction in residual error deviation when measured peak errors are only 25% larger than the deviation of all errors. However, this situation is not likely in practical scanners. To predict expected sidelobe errors then, one should choose probable values of residual position error, based on the actually measured and compensated peak error, and then use these values in equation (5, 7). An example follows.

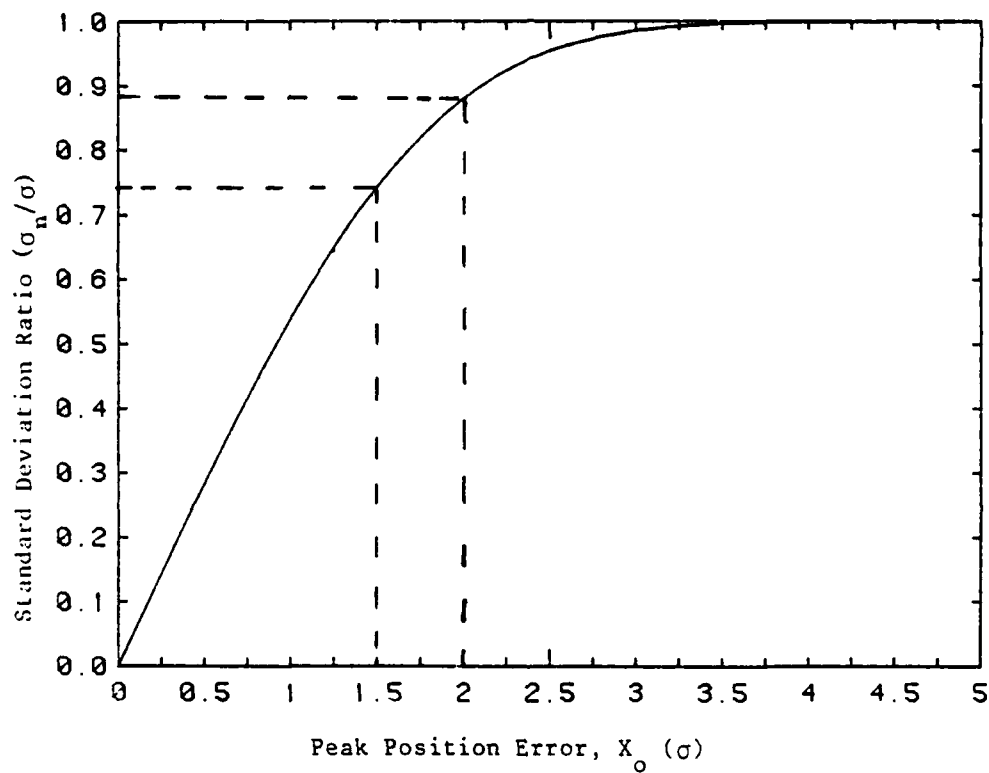


Figure 7. Normalized Standard Deviation of Truncated Gaussian Density for Modeling Residual Probe Position Errors Following Phase-only Compensation

From the curve in Figure 7, if an uncompensated peak Z-position error of value  $X_0 = 2\sigma$ , was observed among all the measured position errors in the scan plane, then the residual error deviation is reduced to  $.89\sigma$ . This residual deviation may be used in equation (7a) to predict the maximum sidelobe error bound with 65.6% confidence.\* Higher confidence sidelobe error bounds may be estimated from other less probable values of residual position error, and of course a 100% confidence bound is estimated from equation (7a) when  $\Delta_p = 2\sigma$ , the truncation point. This residual error-bound procedure is a useful improvement for low sidelobe performance estimation, and is a more practical method for specifying design criteria for the NF scanner.

### 3.2 Multipath Effects

#### 3.2.1 General

Both Newell and Yaghjian have considered the degrading effects of NF multiple reflections on the transformed spectrum of arbitrary test antennas. Both studies have applied analytic techniques to estimate (although very pessimistically) FF sidelobe error from easily measured NF interference magnitudes. The primary interference mechanism is the nearly normal multiple round trip paths between the moving probe and the array face. Of course oblique reflection geometries are possible but well designed scanners can make these interferences nearly insignificant. However, the normal probe/array reflection effects are always present, and represent a fundamental limit to the achievable accuracy of planar NF testing for low sidelobe antennas.

#### 3.2.2 Purpose

Kerns has completed a NF scattering matrix theory of antenna-antenna interactions, which does allow for multiple round trip reflections between probe and array [13]. However, no practical implementation of

---

\*  $\Pr \{ x - U_0 \leq .89\sigma \} = \int_{-.89\sigma}^{.89\sigma} f_1(x) dx = .656$

this complete theory has yet been accomplished. Consequently, the degrading effects of multipath-induced NF measurement error is called acceptable if it can be shown that unavoidable reflection magnitudes are below some specified level. The purpose of this section is to reconsider the existing analysis upon which these reflection magnitude specifications are based. In this way the utility of the bound can be verified, and possible experiments can be suggested to certify its accuracy for low sidelobe testing problems.

### 3.2.3 Multipath Mechanism

The effects of nearly normal probe/array multipath is shown in Figure 8. The curves show NBS-measured relative probe output as a function of increasing probe/array Z-separation, for three probe reference locations in the scan plane. The multipath-induced ripples which have a period of about  $\omega = \lambda/2$  is the observable in this analysis. The peak-to-peak magnitude of one ripple period (indicated as  $\epsilon^{mr}$ ) is transformed into possible FF sidelobe error as shown in equation (18) below. Unless the NF is complicated by blockage effects (usually never the case for a planar array),  $\epsilon^{mr}$  is due only to NF multipath phase change across the measurement area. By comparing several NF scans, made at slightly different separation distances, an estimate of the error sidelobe direction may also be predicted e.g. as illustrated in Figure 9 from Newell [7]. This curve is a plot of the difference between two NF amplitude scans made at  $\lambda/8$  separations. The ripple period  $T_m$  is due to the unique probe/array multipath phase change.

From Figures 8, 9, both the direction and magnitude of the FF sidelobe error can be estimated in the worst case as

#### Sidelobe Error Magnitude

$$\eta^{dB} = 20 \log(1 + \eta(r)) \quad (18)$$

where  $\eta(r) = g(\theta, \phi) \epsilon^{mr}$

with  $g(\theta, \phi) =$  inverse error-free pattern

$\epsilon^{mr} =$  defined from Figure 8 data

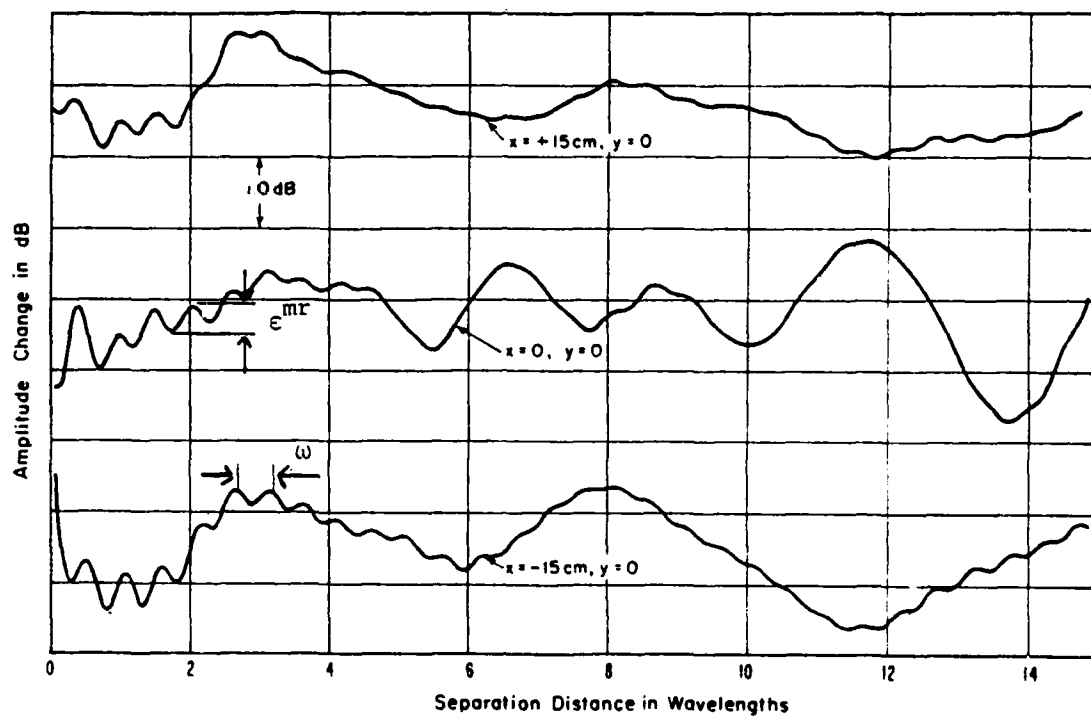


Figure 8. Measured Z-dependent NF Amplitude for Three Reference Locations in the Scan Plan Showing the Peak Interference Magnitude  $\epsilon^{mr}$  Occuring with Period  $\omega = \lambda/2$  due to Probe/Array Multipath [Ref. 7]

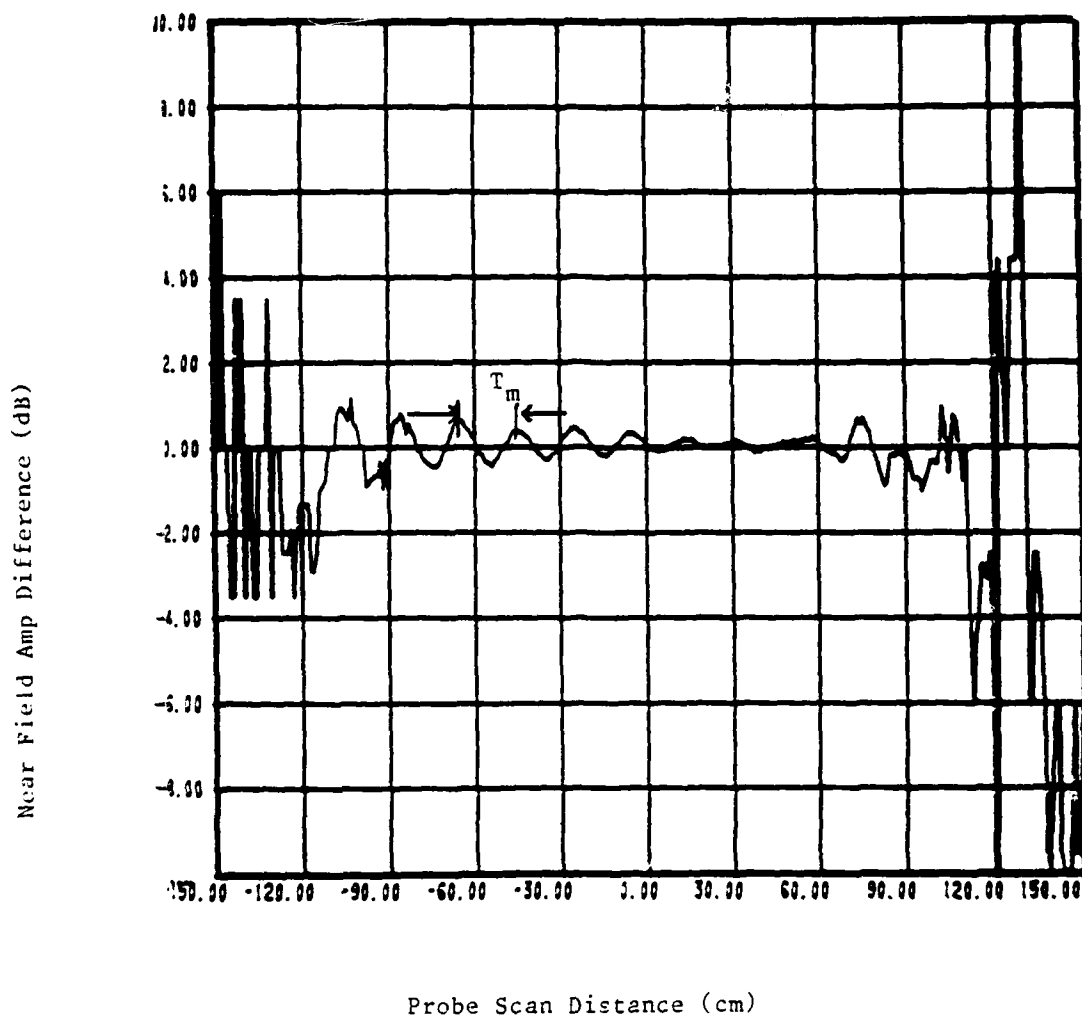


Figure 9. Measured NF Amplitude Difference for Centerline Scans Separated in Z by  $\lambda/8$ . The Ripple Periodicity ( $T_m$ ) is Used to Estimate FF Side-lobe Error Angle [Ref. 7]

#### Sidelobe Error Direction

$$\theta = \sin^{-1}(\lambda/T_m) \quad (19)$$

where  $\lambda$  is RF wavelength

In what follows the above error magnitude estimate is reconsidered for low sidelobe arrays.

#### 3.2.4 Present Error Bound

The existing error bound in equation (18) predicts a worst-case sidelobe error, but this bound is known to be excessive in most practical applications. Its value depends upon the exact nature of the NF phase in the multiply reflected signal. For example, if an arbitrary test antenna is subjected to an interference environment where  $\epsilon^{mr} \approx .01$  (multiple reflections down 40dB), then equation (18) predicts a worst case -30dB sidelobe error of

$$\begin{aligned} \eta_{-30}^{dB} &\leq \pm 20 \log (1 + .01(31.62)) \\ &\leq \pm 2.4 \text{ dB} \end{aligned}$$

However this error will occur only when the multiply reflected NF phase is nearly uniform in the scan area. To test the sensitivity of the bound to realistic phase properties of reflection fields and to the design illumination of the test array, the following numerical exercise has been performed. The goal of the exercise is to find a scale factor for the critical parameter  $\epsilon^{mr}$  in equation (18), such that a more realistic error bound may be found for low level sidelobes.

3.2.4.1 Modified Bound for Uniform Aperture. Assume the planar reflection fields remain linearly polarized upon scattering and have the functional form:

$$\Delta E^{mr} = \epsilon^{mr} E_0 e^{i2\pi \left( \frac{x}{\lambda_1} + \frac{y}{\lambda_2} \right)} \quad (20)$$

where  $E_0$  is the uniform error-free NF amplitude  
 $\lambda_1, \lambda_2$  are arbitrary reflection phase constants  
 $x, y$  are probe scan directions  
 $\epsilon^{mr}$  is the measured interference ratio magnitude  
 We seek the standard Fourier error field transform, given as

$$\Delta E = [\cdot] \int_A \Delta E^{mr}(x, y) e^{-\frac{ik}{r} R \cdot P} dP \quad (21)$$

where  $[\cdot]$  is an error-free radiation kernel  
 $R, r$  are source and field radial directions  
 $P$  is probe transverse  $(x, y)$  location  
 $A$  is the scan area

As used by Yaghjian, the integral in (21) is written in computable polar form as

$$I = \epsilon^{mr} E_0 \int_0^{2\pi} \int_0^a p' dp' d\phi' e^{\frac{i2\pi p'}{\lambda} [\lambda/\lambda_1 \cos \theta' + \lambda/\lambda_2 \sin \phi' - \sin \theta \cos(\phi' - \phi)]} \quad (22)$$

where the prime denotes integration variables. Using the Bessel integral, equation (22) reduces to

$$I = 2\pi \epsilon^{mr} E_0 \int_0^a J_0\left(\frac{2\pi pB}{\lambda}\right) p' dp' \quad (23)$$

where the bracketted exponent in (22) has been written as  $B \cos(\phi' - b)$ , with

$$B = \sqrt{(\lambda/\lambda_1 - \sin \theta \cos \phi)^2 + (\lambda/\lambda_2 - \sin \theta \sin \phi)^2}$$

$$b = \tan^{-1} \left\{ \frac{\lambda/\lambda_2 - \sin \theta \sin \phi}{\lambda/\lambda_1 - \sin \theta \cos \phi} \right\} \text{ for the purposes of } \phi' \text{ integration.}$$

With these substitutions, (23) becomes

$$I = \lambda a \epsilon^{mr} E_0 \frac{J_1(2\pi aB/\lambda)}{B} \quad (24)$$



Now, the desired fractional error ratio  $\eta = \Delta E/E$  is found from (24) and the value of the error-free far field, which for a circular uniform aperture in polar coordinates integrates simply as

$$E_{\text{error-free}} = E_0 \frac{a}{r} (\cos^2 \theta + \sin^2 \theta \cos 2\phi)^{1/2} \left| \frac{J_1 \left( \frac{2\pi a}{\lambda} \sin \theta \right)}{\sin \theta} \right| \quad (25)$$

Using an envelope approximation for  $J_1$  in (25), the desired result is

$$\eta = \frac{e^{mr} \sin \theta \left| J_1 \left( \frac{2\pi a B}{\lambda} \right) \right|}{B (\cos^2 \theta + \sin^2 \theta \cos 2\phi)^{1/2} J_1^{\text{env}} \left( \frac{2\pi a}{\lambda} \sin \theta \right)} \quad (26)$$

#### INTERPRETATION

We wish to plot the fractional error bound  $\eta$  in a single pattern plane (i.e., as a function of single angle variable) for a given size aperture, and for various possible multipath NF phase changes. Thus, set  $\lambda_1 = \lambda_2 = \lambda_0$ , choose  $\phi = 0$  and rewrite  $B = \sqrt{2 \lambda / \lambda_0} (\lambda / \lambda_0 - \sin \theta) + \sin^2 \theta$  such that the final sidelobe error bound becomes

$$\eta(\theta) = \frac{e^{mr} \sin \theta \left| J_1 \left( \frac{2\pi a}{\lambda} B \right) \right|}{B J_1^{\text{env}} \left( \frac{2\pi a}{\lambda} \sin \theta \right)} \quad (27)$$

A mistake in the original Yaghjian expression for (27) incorrectly approximated  $J_1(z)$  for  $|z| < 2$  with the envelope function,  $\frac{z}{2} - \frac{z^2}{8}$ . It should rather be correctly written as  $J_1^{\text{env}}(z) \approx \frac{z}{2} - \frac{z^3}{16}$  for  $|z| < 2$ . This correction has been made to (27) and then plotted for an assumed aperture and six possible values of multipath phase error given by  $a/\lambda_0 = 0.1, 0.3, 1.0, 2.5, 5.0$ , and  $8.0$ . These curves are shown in Figure 10 for a  $12\lambda$  aperture. From the figure, when the multipath-induced phase change across the scan plane is nearly constant ( $a/\lambda_0 < 1$ ), the envelope of the FF error ratio approaches  $e^{mr}$  throughout the sidelobe region, but peaks at about  $1.7e^{mr}$  in the near-in sidelobes. When the NF multipath phase error is moderate ( $a/\lambda_0 \approx 1$ ), the FF error envelope approaches  $e^{mr}$  more slowly, and when the NF multipath phase change is large ( $a/\lambda_0 > 1$ ), the envelope of FF sidelobe errors is small and never exceeds  $.6e^{mr}$  throughout the whole plotted sidelobe

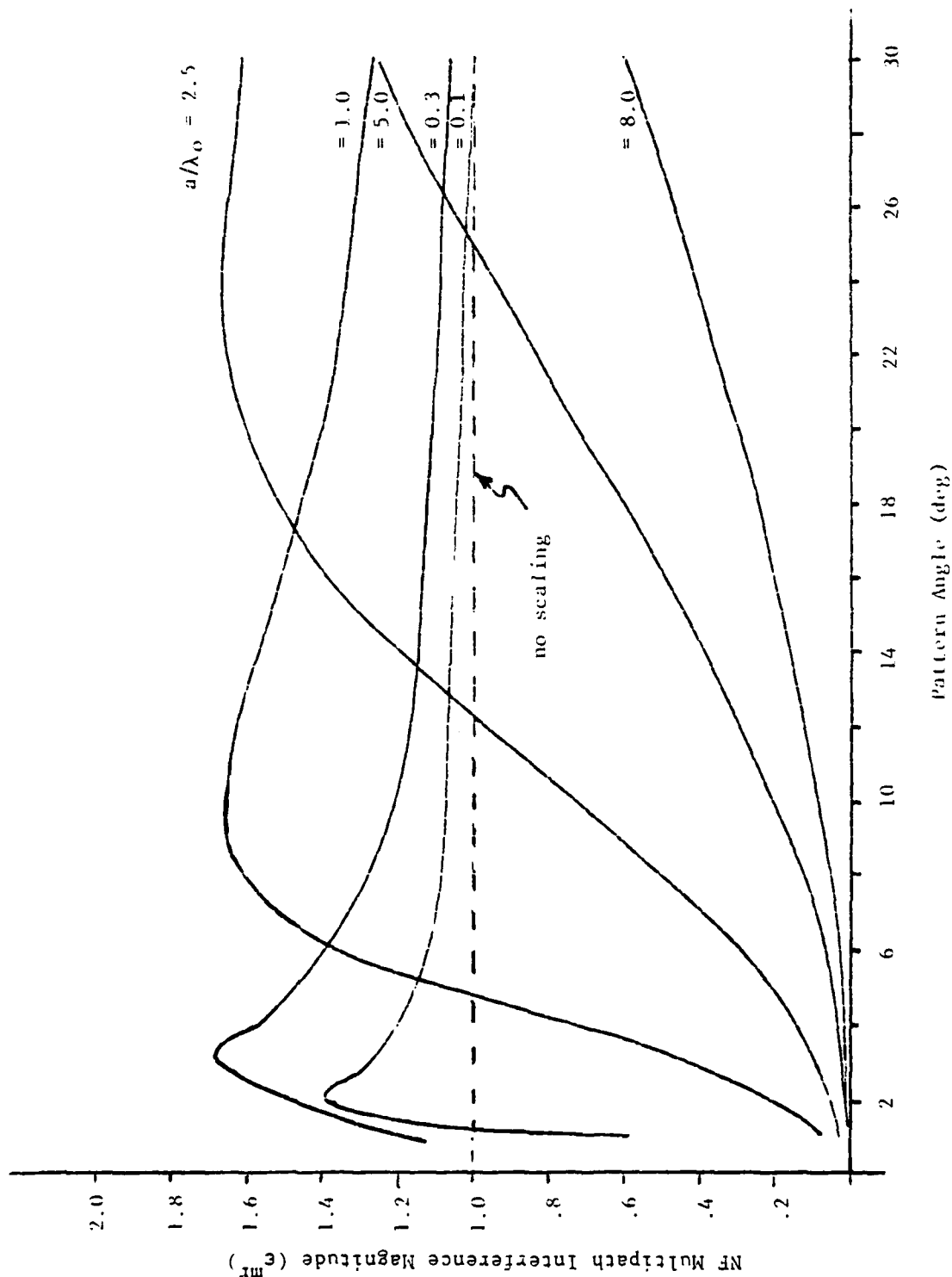


Figure 10. Computed Interference Ratio Scalings for Modifying the Upperbound Error Ratio of a Uniform Aperture Having Various Assumed NF Phase Changes Due to Probe/Array Multiple Reflection

region. These results show the sensitivity of the existing error bound to measurable NF phase change, and are useful for selecting a scaled value of  $\epsilon^{mr}$  to use in equation (18). The same scaling is sought next for a tapered (low sidelobe) aperture.

3.2.4.2 Modified Bound for a Tapered Aperture. A procedure analogous to the example just shown is followed for the low sidelobe case, by including a NF taper factor to account for an arbitrary symmetric aperture illumination. Thus, the assumed multipath error fields are again of functional form

$$\Delta E^{mr} = \epsilon^{mr} E_0 \cos^n(\alpha p') e^{i2\pi(x/\lambda_1 + y/\lambda_2)} \quad (28)$$

where the NF amplitude is tapered by  $\cos^n(\alpha p')$  within the projected aperture on the scan plane ( $|p'| < a$ ), and zero outside. As for the uniform case, we seek the far error field integral

$$I = \epsilon^{mr} \int_0^{2\pi} \int_0^a p' dp' d\phi' \cos^n(\alpha p') e^{\frac{i2\pi c p'}{\lambda}} \quad (29)$$

Note that (29) differs from (22) only by the  $\cos^n(\alpha p')$  term, with  $c$  the bracketted part in the exponent of (22). A standard numerical integration of equation (29) yields the set of results shown in Figure 11. The NF taper factor was assumed to be  $\cos^n(\alpha p')$  for  $n = 1, 2, 3$ , but only a single value of NF multipath phase error ( $a/\lambda_0 = 1$ ) was assumed. In general, the more tapered is the NF, the larger the sidelobe error bound becomes, but interestingly only for the near-in sidelobe region. This data again assumes a  $12\lambda$  aperture as in the previous example. Figure 11 also shows that the sidelobe error bound approaches the same limiting value of  $.35\epsilon^{mr}$  for all three tapers evaluated, since only a single NF multipath phase error value was assumed. This demonstrates that predicted sidelobe error for a low sidelobe illumination will have a smaller maximum bound than presently specified by equation (18), but only in the far out sidelobe region. Conversely, the nearer-in sidelobes are predicted to be in larger error than previously estimated, but of course the actual value

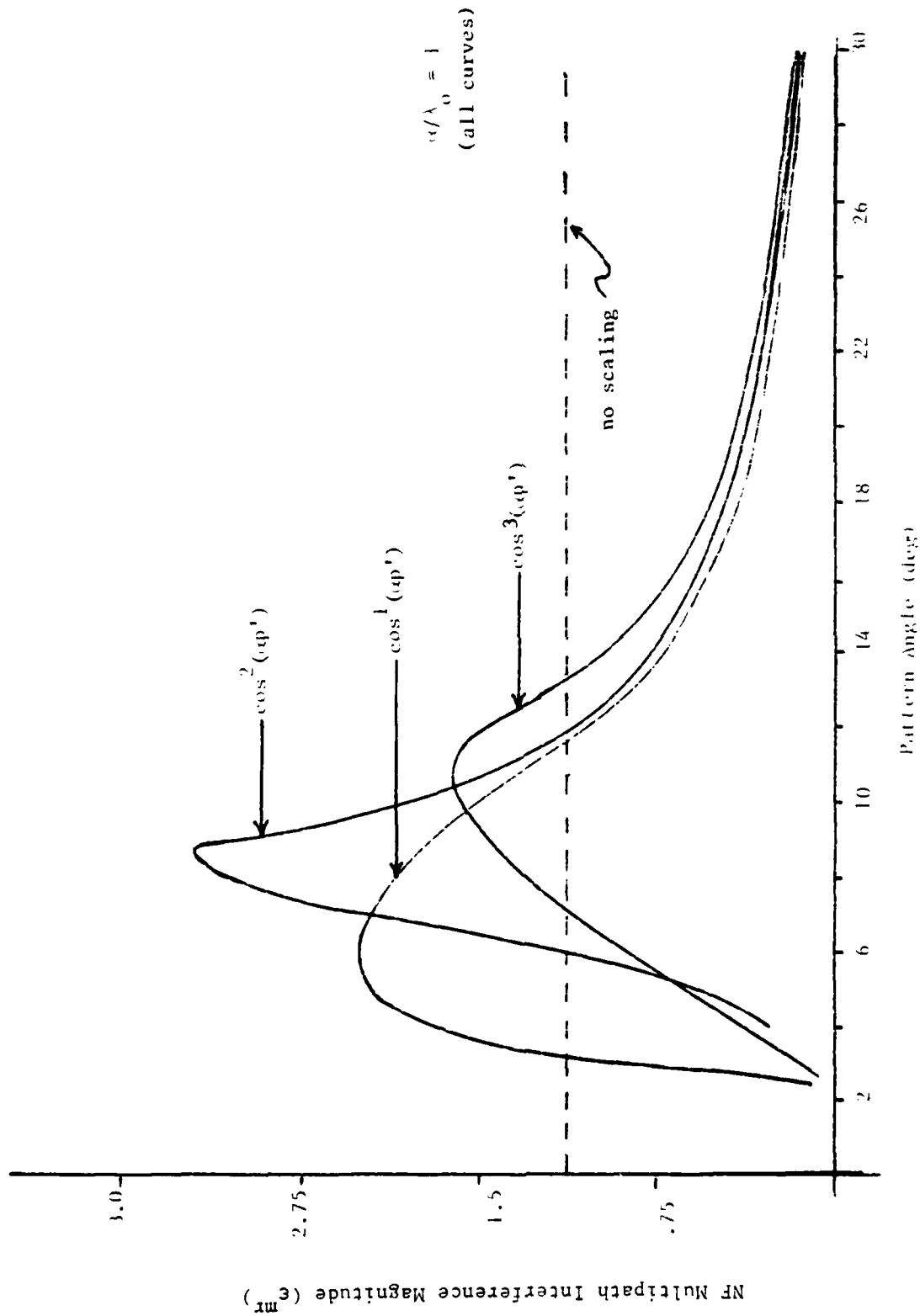


Figure 11. Computed Interference Ratio Scalings for Modifying the Upperbound Error Ratio of a Tapered Near Field Having a Single NF Phase Change ( $a/\lambda_0 = 1$ ) Due to Probe/Array Multiple Reflection

will depend upon the actual NF taper and the measured NF multipath phase error. It is thus quite important to measure not only the peak NF interference ripple magnitude as in Figure 8, but also to measure or estimate the NF multipath-induced phase error across the scan plane. From the latter, a scale factor can be found to modify the critical parameter  $\epsilon^{mr}$ , and consequently to improve the FF error estimation on very low sidelobes. For this exercise, the scaling factor for  $\epsilon^{mr}$  was in the range  $.35 < k < 2.7$ . Scaling factors will depend upon both the degree of NF taper and the measured NF phase error with scan. Such measurements will be performed and summarized parametrically for a qualified low sidelobe array during the DESAT phase 2 program.

During the course of this study, several new NF probing concepts have been considered for possible application to low sidelobe testing problems, and are listed in Table 2 along with rationale comments. In this section, only concepts 2,3, and 4 are discussed, as these are considered most practical for continued development during the phase 2 DESAT program. Technique #5, position error correction, was discussed in Section 3.1.

## 4.1

Reduced Scattering Probe

It has already been shown in Figure 8 that nearly normal scattering between NF probe and array face is responsible for NF interference effects whose peak magnitude  $\epsilon^{mr}$  is a fundamental measurement limitation for low sidelobe testing. A method to more accurately estimate sidelobe error by incorporating an error bound scale factor for  $\epsilon^{mr}$  was developed in Section 3.2. Now it is desired to absolutely reduce  $\epsilon^{mr}$  by seeking a probe design which has an inherent lower scattering cross section. It is suggested that a reduced-scattering probe might result if it were equipped with adjustable termination. The termination would present a slight mismatch, capable of minimizing its scattered field, and consequently, the resulting NF interference peaks, to some acceptable level.

## 4.1.1

Probe Scattering Cross Section

Kraus [14] has defined the scattering aperture of an antenna as the ratio of the re-radiated power to the power density (P) of the incoming wave, i.e.,

$$A_s = \text{scattering aperture}$$

$$= \frac{V^2 R_r}{P (R_r + R_L + R_T)^2 + (X_A + X_T)^2} \quad (30)$$

where

V is the probe load voltage

$R_r$ ,  $R_L$ ,  $R_T$  are resistances of the probe's radiation, loss and load

$X_A$ ,  $X_T$  are probe and load reactances

Table 2. Possible Improved PNF Probing Concepts  
for Low Sidelobe Array Testing

Probing Technique	Rationale
1. Amplitude-only (multiple probes)	<ul style="list-style-type: none"> <li>- eliminate need to measure NF phase</li> <li>- possible recovery of NF phase from multiple-probe amplitude data prior to FFT</li> </ul>
2. Reduced-Scattering Probe	<ul style="list-style-type: none"> <li>- minimize nearly perpendicular array/probe scattering</li> <li>- replace existing multiple-plane data averaging compensation procedure</li> </ul>
3. Optimum Probe Design	<ul style="list-style-type: none"> <li>- find a probe(s) which is most responsive to test array's sidelobe spectrum</li> </ul>
4. Minimum Sampling	<ul style="list-style-type: none"> <li>- greatly reduced data acquisition/processing burden</li> <li>- acceptable "additional" error in low sidelobe testing problems</li> <li>- remote-site, i.e., low cost simple, scanner design possible</li> </ul>
5. Probe Position-Error Compensation	<ul style="list-style-type: none"> <li>- remove scanners "as-built" systematic positioning error</li> <li>- probable sidelobe error related to residual position error statistics</li> </ul>

Under conditions of maximum probe power transfer, i.e., the probe having a matched load for which  $R_L = 0$ ,  $R_T = R_r$  and  $X_A = -X_T$ , then  $A_s$  becomes

$$A_s = \frac{V^2}{4PR_r} \quad (31)$$

$A_s$  is also known to be equal to the maximum effective probe aperture,  $A_e$ . Thus the maximum power in the probe terminals is equal to the power reradiated or scattered back to the array.

By increasing the probe's terminal resistance, both the scattering and effective aperture cross sections are decreased, although  $A_s$  does so more quickly as shown in Figure 12, which plots (30) for several  $R_T/R_r$  ratios for a lossless probe when  $X_T = X_A = 0$ .

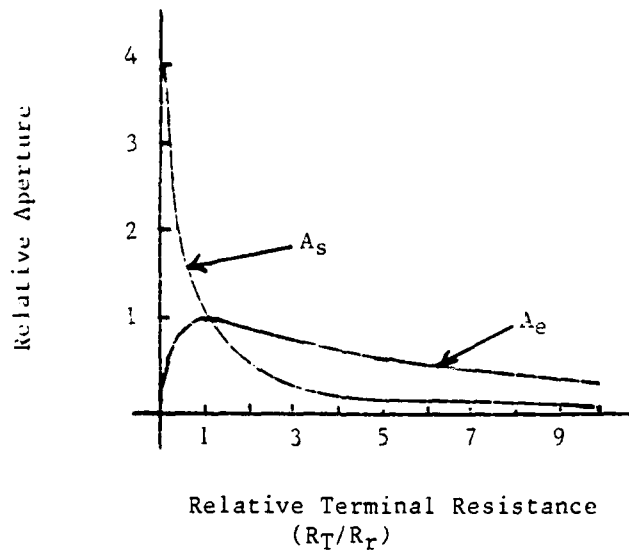


Figure 12. Relative Scattering ( $A_s$ ) and Effective ( $A_e$ ) Probe Cross Sections as a Function of Load Resistance. The maximum Effective Aperture Occurs for the Matched Load  $R_T/R_r = 1$  [Ref. 14, p. 47]



Figure 12 shows that the scattering cross section of the probe can be reduced about 50% by doubling the terminal resistance, while only decreasing its effective aperture to 90% of its maximum value. Such a resistive load might then reduce probe scattering (i.e., reduce  $\sigma_{mr}$ ) to acceptable levels for accurate low sidelobe testing. Ways to minimize the inherent probe scattering cross section will be proposed during the phase 2 program. They will include match technique as described herein, and possible dielectric loading to minimize the probe physical aperture.

#### 4.2 Minimum Sampling Schemes

In addition to the basic measurement error sources listed in section 1.4, low sidelobe accuracy also depends on acquiring NF data of sufficient density and extent so as to not introduce aliasing or other sampling error into the computed spectrum. These basic sampling criteria have been long established and derive from the usual Fourier processing constraints\*. However these constraints usually lead to burdensome data acquisition requirements, even for moderate-size arrays. In this section, an alternate data acquisition/processing scheme is proposed which significantly reduces this burden, while still preserving the sidelobe measurement accuracy. The algorithm, called "Collapse," is based on a highly thinned sampling strategy.

##### 4.2.1 Collapse Pattern Processing

Collapse sampling has been developed when simple scanners are sought, or when the cost of data acquisition/processing is a principal testing concern. Its use with moderately low sidelobe arrays has been demonstrated in Air Force applications [15]. The chief advantage of Collapse is that principal FF patterns are easily, quickly, and accurately transformed from highly thinned measurement data. Its principal disadvantages are that data reacquisition is required should a second FF pattern plane be required, and that beam gain is inaccurately found. However, recent studies have addressed

---

\* The recertification of these basic sampling criteria (e.g., scan length and sample density for selected separations) is a first goal of the DESAT phase 2 demonstration.

this latter disadvantage by incorporating a data processing technique which extrapolates the thinned NF data [16]. This section examines the accuracy of Collapse processing on sidelobe levels using Navy owned NF array data.

#### 4.2.2 Collapse Algorithm

A rectangular grid of PNF samples is sketched in Figure 13 with a standard rectangular coordinate system also shown. The grid of data is assumed to have adequate extent and density as if Fourier processing were intended. The ability of Collapse to process only selected rows of the dense data is shown as follows. From simple array theory, the field at any point  $P(\theta, \phi)$  is:

$$P(\theta, \phi) = \sum_m \sum_n A_{mn} \exp[2\pi j(d_{xn}\psi_x + d_{ym}\psi_y)] \quad (32)$$

where  $A_{mn}$  =  $mn^{\text{th}}$  NF sample  
 $d_{xn}$  = x distance ( $\lambda$ ) of  $n^{\text{th}}$  sample from ref ( $= n\Delta X$ )  
 $d_{ym}$  = y distance ( $\lambda$ ) of  $m^{\text{th}}$  sample from ref ( $= m\Delta Y$ )  
 $\psi_x = \sin \theta \cos \phi$   
 $\psi_y = \sin \theta \sin \phi$  } direction cosines

The collapsed NF is found from (32) by fixing  $\theta$  or  $\phi$  and performing the inner summation in order to reduce the two dimensional NF into an equivalent linear NF. For example, selecting  $\phi = 90^\circ$  specifies the principle horizontal pattern (yz plane) and collapses the PNF as

$$P(\theta, 90^\circ) = \sum_m \left\{ \sum_n A_{mn} \right\} e^{j2\pi d_{ym}\psi_y} \quad (33)$$

one of the  $m$  elements in the collapsed NF

This expression may then be evaluated by indexing over  $m$  for a selected range and resolution on  $\psi_y$ , i.e., for arbitrary pattern field of view and pattern smoothness. The resulting yz plane pattern is then the FF pattern sought. Errors introduced by thinning the measured PNF in the  $n$  index (i.e., along the rows) may be determined by excluding some of the rows during the collapse, computing the resulting pattern, and then comparing it to the full data pattern.



Such an exercise was undertaken using Navy-owned PNF data as described next.

#### 4.2.3 Collapse Results

Equation (33) was implemented to process PNF data from a complete two dimensional scan of a Navy-owned array antenna, having only moderate sidelobes. The data included  $n = 181$  rows of  $m = 182$  samples each. Sample spacing was  $.32\lambda$  in both dimensions, and the planar scanning region extended sufficiently far beyond the aperture edge to guarantee accurate FF patterns over at least a  $\pm 52^\circ$  field of view (see equation 3). This complete NF data set of 32942 complex measurements was thinned by deleting successive rows (by powers of 2), and computing the resulting thinned pattern for comparison to the full data set pattern. RMS and peak sidelobe errors for five such thinning ratios are tabulated in Table 3. Figure 14 shows these patterns overlayed as the light trace for each of the thinning ratios. The pattern plotted as the dark trace is due to the complete (unthinned) NF data. The last column in Table 3 gives the RMS errors of difference between unthinned and thinned pattern.

Table 3. Summary of Additional Pattern Error Due to Collapse Processing of Navy-owned PNF Data For a Moderate Sidelobe Array.

Thinning Ratio	Peak Error at level (dB)				Sidelobe RMS	Error Pattern RMS
	-25	-30	-40	-50		
1.0 (No Thinning)	-	-	-	-	-36.99dB	-
.5	0	0	1.0	4.5	-37.00	-66.23 dB
.25	0	2.0	1.2	6.2	-36.07	-53.13
.125	0	4.0	6.3	8.6	-35.56	-49.90
.0625	3.2	4.8	7.25	10.1	-34.46	-46.02
.03125	6.1	7.2	8.6	12.5	-32.17	-40.01

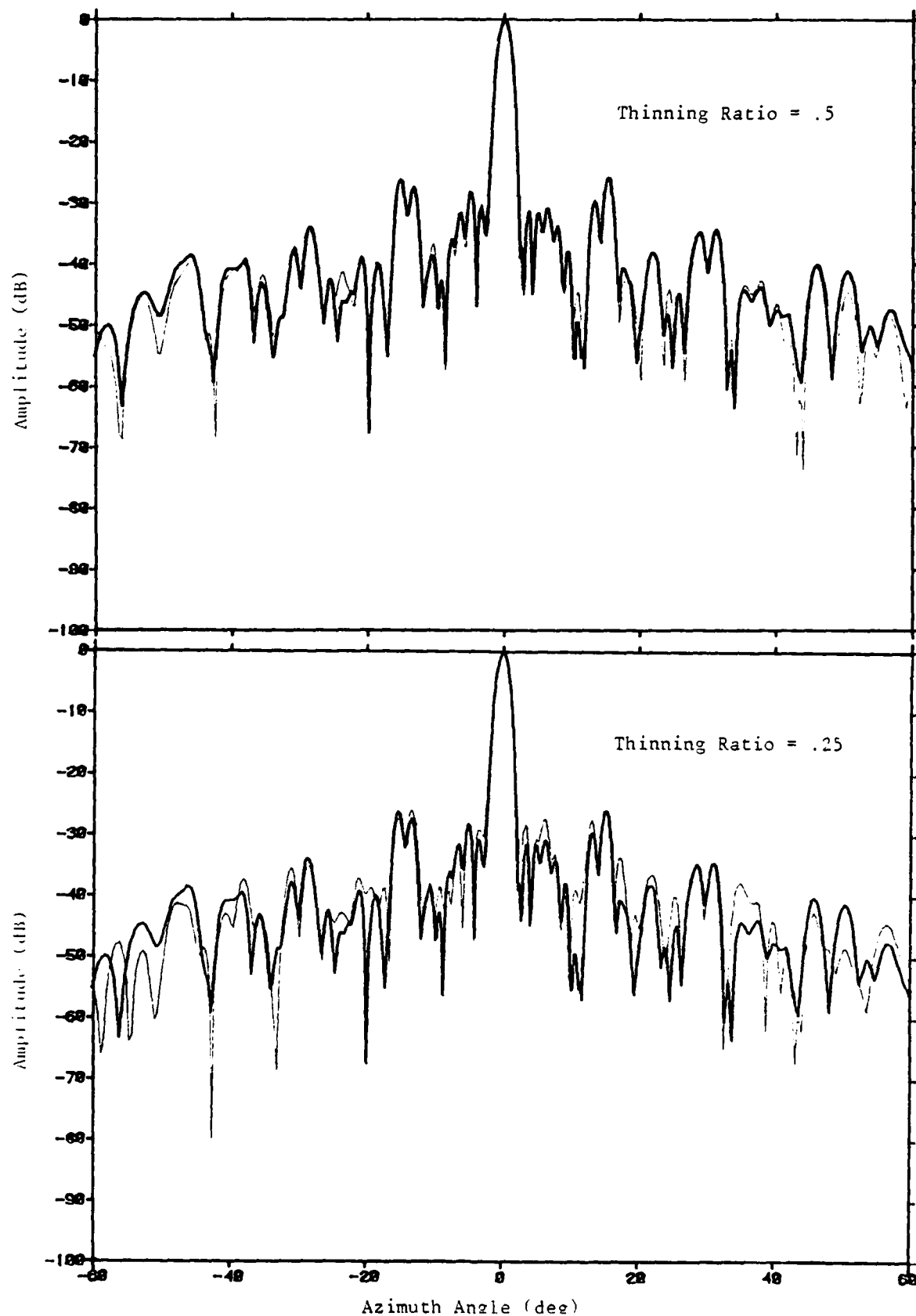


Figure 14. Collapse-processed YZ Plane Pattern for Full PNF Data Set (Dark Curve) and for Various Thinning Ratios (Light Curve) for a  $44\lambda$  Moderate Sidelobe Array

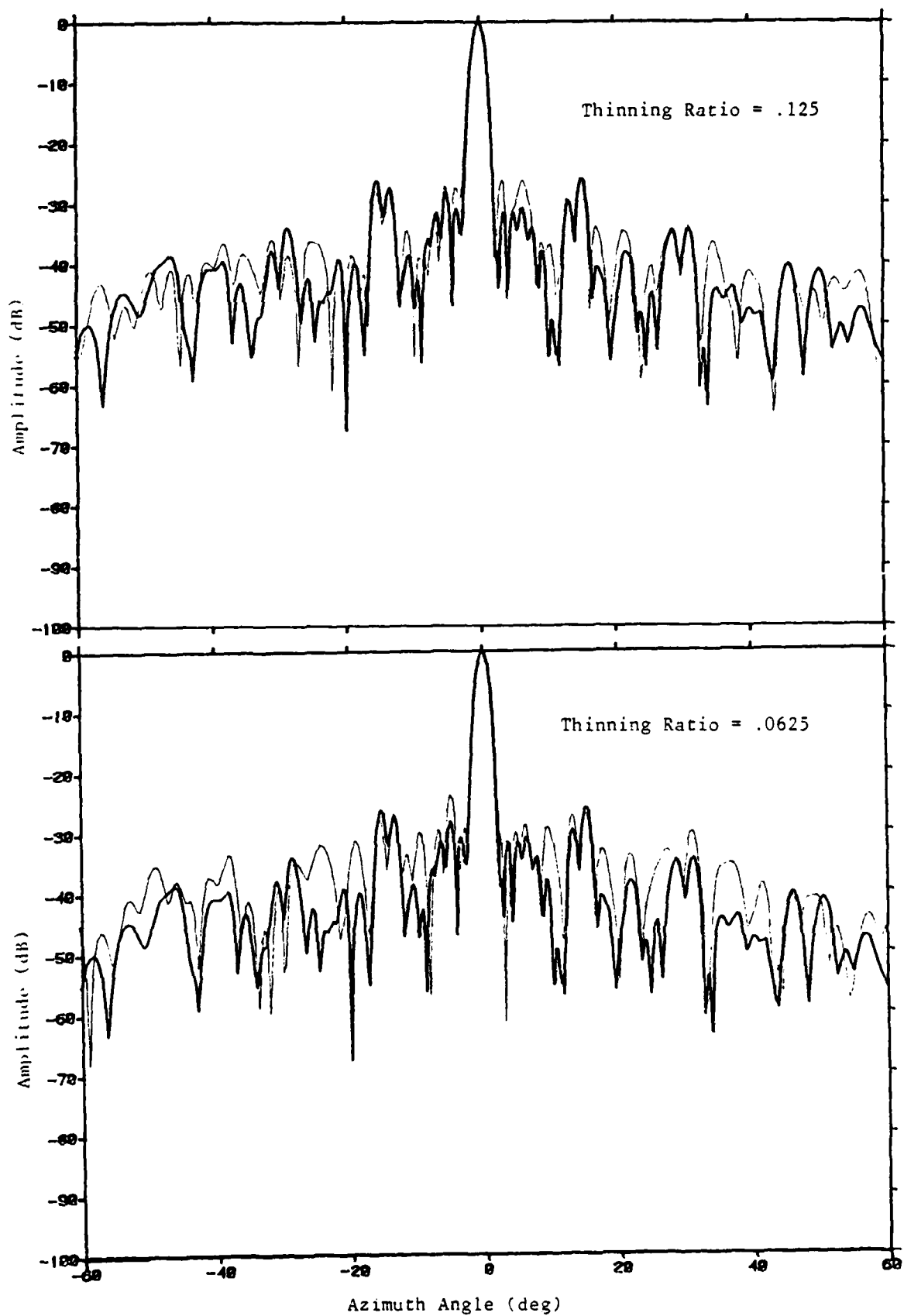


Figure 14. (continued) Collapse-processed YZ Plane Pattern for Additional Thinning Ratios

The table indicates that if only the principal  $\alpha$ -plane pattern (yz plane in Figure 13) is sought from a limited PNF test, then no more than 12.5% of the full set normally acquired for Fourier processing need actually be measured. For such thinning (ratio = .125 in table 3) only 23 of 181 usually acquired scans need actually be measured. Then, the additional pattern error will increase the sidelobe RMS by 1.43 dB and generate peak errors of 6.3 dB at the 40 dB sidelobe. Such degradations may be acceptable in some applications, however.

4.2.1.1 Utility. Minimum sampling schemes as Collapse are most advantageous if simple linear scanners are to be designed which automate probe motion in only the scan dimension. The manual effort to reposition the entire scanner in the step direction could be endured if only a few such repositions were necessary. Thinned PNF sampling would make possible remote-site or even on-ship array testing, if a reasonable mechanical design could be developed. Such a design is beyond the scope of the present DESAT study, however the utility of the minimum-scan concept, as shown here for a moderate sidelobe array, will be demonstrated for a low sidelobe array during the DESAT phase 2 program.

### 4.3 Optimum Probes

#### 4.3.1 Existing Criteria

Huddleston has rigorously given design criteria for an "optimum" PNF probe [17]. A "best-pattern" probe can be specified when scanning over a finite measurement region, and when testing an array whose measured spectrum,  $\hat{A}(k_x)$ , is to have a minimum Mean Square Error (MSE) with respect to the true spectrum,  $A(k_x)$ , i.e.,

$$\min (\text{MSE}) = \min \int_{-k_{\max}}^{-k_{\max}} |A(k_x) - \hat{A}(k_x)|^2 dk_x \quad (34)$$

A non-optimum probe pattern is a fundamental measurement error source when

- the scanner's finite size is indeed restrictive,
- the test antenna radiates significant field strength at the edge of the scan plane, and
- wide-angle FF pattern accuracy is desired.

Since beam scanning arrays can generate large edge fields, and since low side-lobes usually appear at wide angles, the need to describe an optimum low sidelobe PNF probe is a present concern.

#### 4.3.2 Description of Existing Optimum Probe

The present criterion for an optimum probe requires it to maximize the concentration of power in its NF response over the available length of scan, i.e., its NF response should satisfy



$$\frac{\int_{L_x} |v(x)|^2 dx}{P_\infty} \triangleq 1 - \epsilon_x^2 \quad (35)$$

where

$P_\infty$  is the total radiated power in the forward hemisphere, and

$\epsilon_x^2$  is a measure of the probe's ability to concentrate its power response, i.e., its directivity.

For the class of waveguide probes considered by Huddleston, the optimality condition in (35) which satisfies the error criterion in (34) has been shown to occur when the probe aperture has a critical E-plane dimension of  $1\lambda$ . The H-plane dimension is less critical, but  $1\lambda$  is also recommended. A summary of Huddleston's design analysis which certifies the optimum waveguide probe dimensions is reprinted in Figure 15 below. The plot shows that the critical E-plane probe dimension of  $b_p = 1\lambda$  produces the smallest unconcentrated response,  $\epsilon_x^2$ , i.e., has the optimum directivity. Such a probe best intercepts the planar near field for all possible scan lengths,  $L_x$ . The relation between  $L_x$  and the plotted coordinate,  $\sin \theta_{\max}$ , is shown in the inset. Values of  $b_p$ , either less than or greater than  $1\lambda$ , produce larger values of  $\epsilon_x^2$ , and hence are suboptimum (MSE sense). Note that this is true only for the class of dominant-mode waveguide probes considered by Huddleston. An alternate class of PNF probes is suggested in section 4.3.3.2. The results in Figure 15 were calculated from the simulated PNF region of a 45 element phased array operating at C-band and steered to  $45^\circ$  in elevation. That  $b_p = 1\lambda$  has the optimal directivity over the available scan length, is shown by simulated PNF data in Figure 16. These curves show that the  $b_p = 1.0\lambda$  probe produces a more concentrated NF response with scan than do either the larger or smaller waveguide probes studied, and hence is the optimum MSE probe for PNF testing.

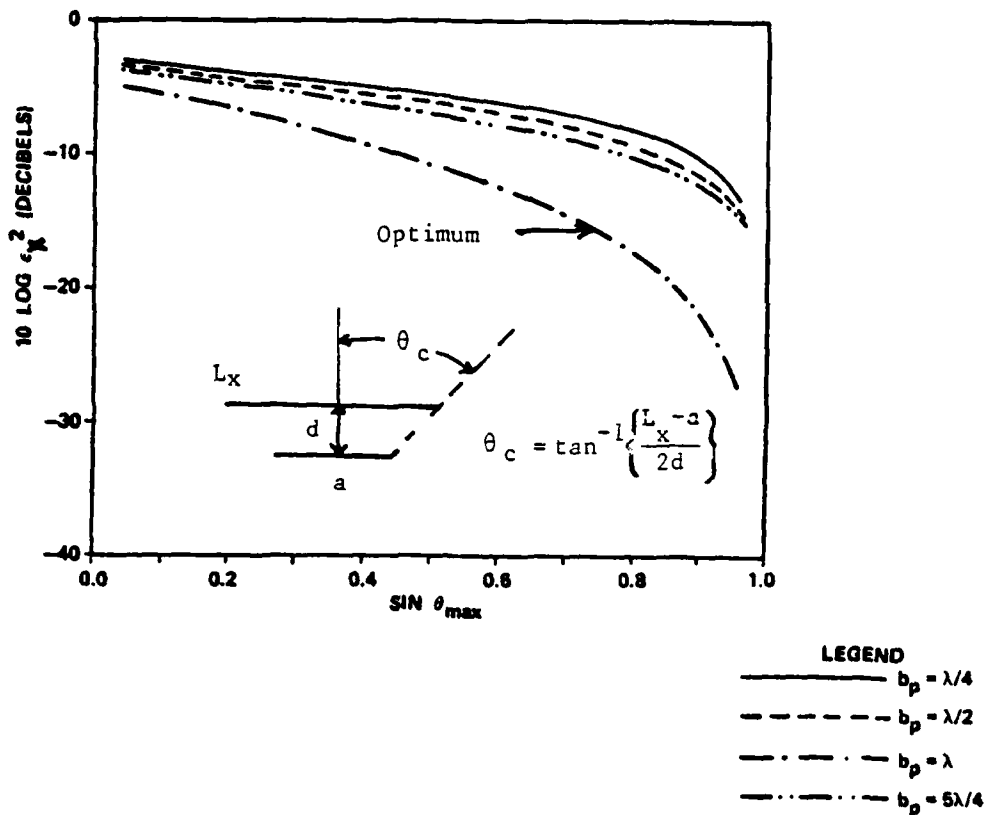


Figure 15. Computed Probe Concentration Factor,  $\epsilon_x^2$  versus  $\sin \theta_{\max}$  for Waveguide Probes Whose Apertures Have Height  $b_p$  When Testing a Simulated Phased Array Scanned to  $45^\circ$  in Elevation. [Huddleston, p. 89] The  $b_p = 1.0\lambda$  Probe is Optimum in a Mean Square Sense.

#### 4.3.3 Alternate Design Criteria for Low Sidelobe PNF Probe

The MSE criterion in equation (34) is obviously dominated by mainbeam contributors, i.e., large errors in the transformed sidelobe spectrum will not appreciably affect the mean square error, but even small errors in the mainbeam spectrum will make large contributions. An alternate probe criterion might lead to alternate probe design for improved accuracy in low sidelobe testing. Such an alternate probe, if it exists, should minimize the weighted MSE, where the weight will be selected to emphasize the sidelobe spectrum. This idea implies that sidelobe and mainbeam spectral errors cannot simultaneously be

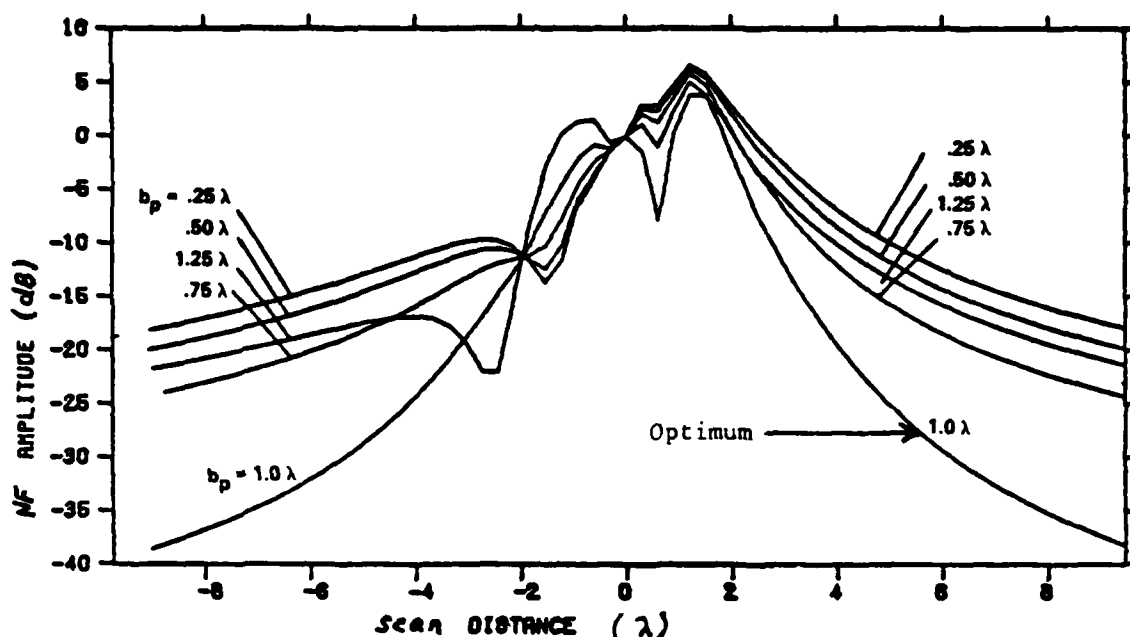


Figure 16. PNF Vertical Scan Response through Peak of Simulated Array Scanned to  $45^\circ$  in Elevation for Various Waveguide Probes. [Huddleston, p. 85] The  $b_p = 1.0\lambda$  is the Simulated PNF Response of the Optimum Probe.

minimized during a single measurement. For improved sidelobe accuracy, we seek a probe (probes) whose PNF response can be processed to minimize a Weighted Mean Square Error (WMSE) criterion, suggested as

$$\min (\text{WMSE}) = \min \int_{-k_{\max}}^{k_{\max}} |W(k_x) [A(k_x) - \hat{A}(k_x)]|^2 dk_x \quad (36)$$

where

$$w(k_x) = \begin{cases} 1 & k_c < |k_x| < k_{\max} \quad (\text{sidelobes}) \\ 0 & 0 \leq |k_x| \leq k_c \quad (\text{mainlobe}) \end{cases}$$

and  $k_c$  is the first zero wavenumber (first null).

Thus,  $W(k_x)$  is a wavefilter which effectively notches out the mainbeam of the test array as sketched in Figure 17. The realizability of this wavefilter for practical probes is next addressed.

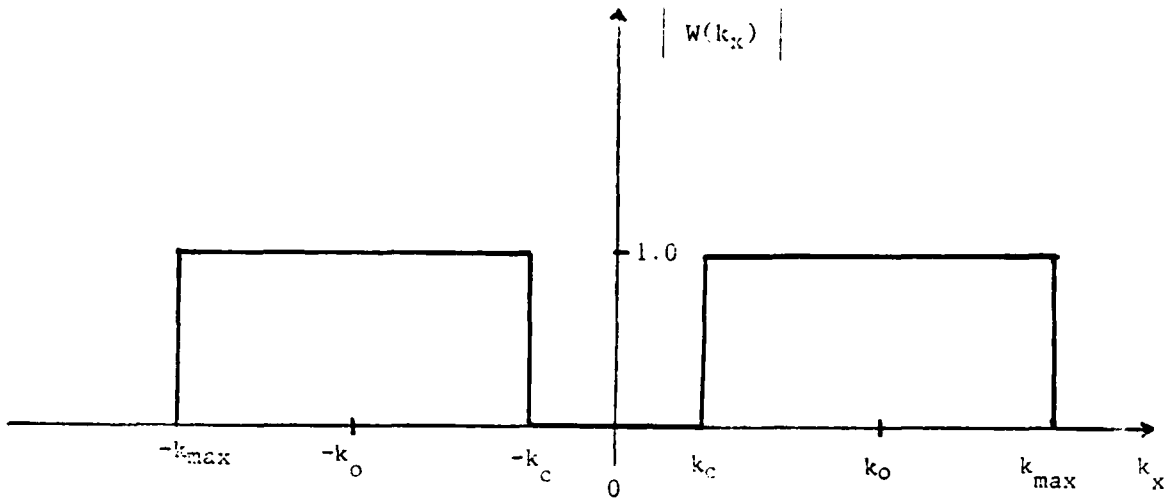


Figure 17. Proposed Alternate WMSE Probe Spectrum where  $|k_{\max}|$  is the Maximum Visible Wave Number, and  $|k_c|$  is the First Zero Wave Number

#### 4.3.3.1 Wavefilter for Optimum Low Sidelobe PNF Probe

The product of the test antenna spectrum and probe spectrum, within the real space window ( $|k_x| \leq k_{\max}$ ), must possess the bandstop shown in Figure 17 in order to satisfy the WMSE criterion in (36). That such a bandstop cannot be realized for any of the dominant mode waveguide probes normally used in PNF testing is simply shown.

Write  $W(k_x)$  in (36) as

$$W(k_x) = I_{\Omega}(k_x - k_o) + I_{\Omega}(k_x + k_o) \quad (37)$$

where

$I_{\Omega}(k_x)$  is the standard spectral pulse function, and

$$k_o = (k_{\max} + k_c)/2$$

The Fourier inverse of  $I_{\Omega}(k_x)$  is the well known  $\text{sinc}(x)$  function, and using the Fourier translation theorem, get

$$\begin{aligned} w(x) &= F^{-1} \left\{ I_{\Omega}(k_x - k_o) + I_{\Omega}(k_x + k_o) \right\} \\ &= \frac{\Omega}{\pi} \frac{\sin(x\Omega/2)}{x\Omega/2} \cos k_o x \end{aligned} \quad (38)$$

Noting that  $\Omega = k_{\max} - k_c$ , (38) becomes the sought form of the effective probe aperture voltage, or

$$w(x) = \frac{(k_{\max} - k_c)}{2} \frac{\sin\left(\frac{k_{\max} - k_c}{2}x\right)}{\left(\frac{k_{\max} - k_c}{2}x\right)} \cos\left(\frac{k_{\max} + k_c}{2}x\right) \quad (39)$$

Equation (39) is plotted in Figure 18 where the abscissa coordinate measures the infinite probe aperture extent in units of  $1/k_c$ , where  $k_c$  is the array spectrum 1st zero. The plot appears to require impossible properties of any practical probe, such as

- i) the probe must have a very large aperture and apparently be capable of supporting a multimode illumination which has many zeros and phase changes
- ii) the probe illumination is unique for each mainbeam width array pattern to be tested.

It is concluded that for the class of dominant-mode waveguide probes normally used in PNF testing, there does not exist a probe pattern which is capable of implementing the WMSE wavefilter specified in Figure 17. Consequently, a realizable (approximate) WMSE pattern if it exists, must be generated by a new class of PNF probes.

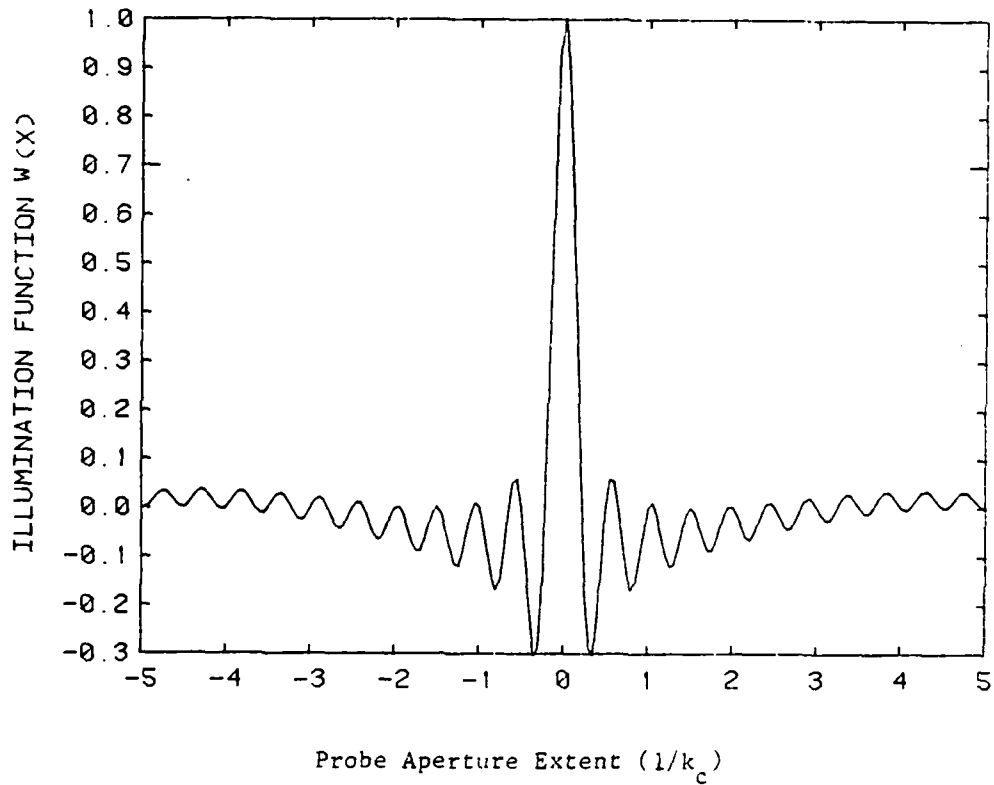


Figure 18. Theoretical Probe Aperture Function Needed to Implement the Mainbeam Bandstop Wavefilter in Figure 17, given in Normalized Aperture Length  $1/k_c$ .

#### 4.3.3.2 Realizable Low Sidelobe Probe

The search for practical probes, which even approximately satisfies the WMSE criterion in equation (36), should be tempered by several physical constraints on realizability. These are suggested to be:

- 1) Minimum scattering cross-section
- 2) Minimum response in direction of mainbeam and maximum response in direction of sidelobes
- 3) Minimum concentration factor,  $\epsilon_x^2$ , i.e., "best" directivity for available scan length
- 4) Not-unique for each possible array pattern to be tested

An alternate class of PNF probes which appear capable of satisfying the above constraints, while at the same time implements the WMSE wavefilter approximately, is the radially responsive, electrically small dipole. Such a probe was suggested by Wacker in 1974 as the best probe for spherical NF scanning [18], and has also been used in practical NF applications by James and Longdon [19]. Radial dipoles respond to the  $E_r$  field component only when used in its near field, i.e., when  $r < 1$ . Then,  $|E_r|$  is proportional to

$$\cos \theta \left( \frac{1}{r^2} + \frac{1}{j\omega r^3} \right) \quad (40)$$

where  $\theta = 90^\circ$  is boresight  
 $r$  is the distance to field point  
 $\omega$  is the RF angular frequency

At the same time, the transverse NF response of a radial dipole is well known, and proportional to

$$\sin \theta \left( \frac{j\omega}{c^2 r} + \frac{1}{cr^2} + \frac{1}{j\omega r^3} \right) \quad (41)$$

Thus, radially responsive probes have a minimum response (notch) in the direction of the test array peak directivity, and simultaneously have a maximum response to the test arrays radial NF. Such a probe must be used in its NF, as well as the NF of the test array.

#### 4.3.3.3 Design Approach for Realizable Probe

The radial dipole just described must be scanned on a plane  $< 1\lambda$  removed from the test array aperture, and even then, its overhead notch pattern is very narrow and hardly matched to a mainbeam width of an arbitrary array. Thus, this new probe class is not a good approximation to WMSE wavefilter sought. A design approach for an improved realizable WMSE probe is as follows. Consider a small probe array of clustered radial dipoles as shown in Figure 19. Here the number of elements  $N$ , their relative spacing  $\Delta s$ , and their complex weight  $b_n$ , are design parameters to be selected by conducting a MSE numerical optimization design study. The resulting transverse FF probe array pattern is to be a best-fit to the optimum WMSE wavefilter, when the probe array is constrained to have the fewest number of dipole elements, the smallest possible spacing, and realizable complex element weights,  $b_n$ .

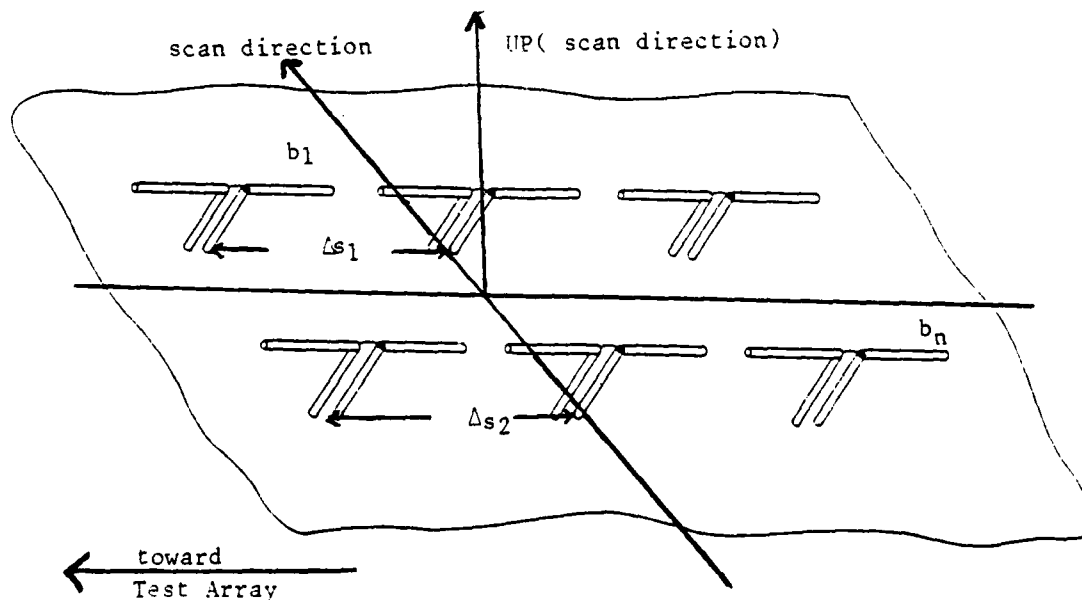


Figure 19. Geometry for Optimization Analysis for Defining the Realizable WMSE Probe



Such a design optimization will be performed, and the probe constructed, during the DESAT phase 2 effort. A summary of the optimization problem, however, serves to establish the feasibility of the design approach as follows.

#### WMSE Probe Design Optimization Summary

- 1) Specify the general planar array probe illumination,

$$v(x) = \sum_{n=0}^{N-1} b_n \delta(x - n\Delta x)$$

- 2) Find the family of probe array patterns from (1) via Fourier Transform,

$$\begin{aligned} B(k_x) &= \mathcal{F}\{v(x)\} \\ &= E(k_x) \sum_{n=0}^{N-1} b_n e^{-in\Delta x k_x} \end{aligned}$$

where  $E(k_x)$  is the elemental pattern.

- 3) Select the specific  $B(k_x)$  which minimizes equation (36) i.e., find  $B(k_x)$  such that

$$\min(\varepsilon) = \min \int_{-k_{\max}}^{k_{\max}} |W(k_x)[A(k_x) - \hat{A}(k_x)]|^2 dk_x$$

$$\text{where } \hat{A}(k_x) = A(k_x)B(k_x)*P(k_x)$$

with \* indicating convolution over the measurement region,  $p(x)$ , subject to the following probe design constraints:

$$\left. \begin{array}{l} N \leq N_{\max} \\ \Delta x \leq \Delta_{\max} \end{array} \right\} \begin{array}{l} \text{constraints size of} \\ \text{probe array} \end{array}$$

$$b_n \text{ realizable}$$

When found, the set of dipoles  $N$  whose planar lattice has element spacing  $\Delta s$ , and whose complex weights are  $b_n$ , will radiate a best approximation to the desired WMSE wavefilter, while simultaneously presenting the smallest scattering cross-section. Selectable overhead null widths, to match an arbitrary test array mainbeam width, may be achieved for selectable weight sets,  $b_n$ . During DESAT phase 2, both a single element radial dipole probe and an optimally-designed probe array cluster, will be used in tests of sidelobe measurement accuracy with a very low sidelobe array.

## 5.0 CONCLUSIONS AND RECOMMENDATIONS

### 5.1 General

This study has extended the existing methods of bounding far field array pattern errors when testing by the method of planar near field probing. Improved error limits have been developed which estimate the low level sidelobe error introduced by probe positioning tolerances and near field multiple reflection. The fundamental measurement error source due to the nature of the probe pattern is shown to be optimally minimized for a new class of probes which simultaneously reduce their own backscatter while providing the maximum sensitivity to the test array sidelobe region. A recommendation is made to design an optimum low sidelobe probe and to conduct a credible testing demonstration using a qualified array and test facility as part of a proposed Defense Small Business Advanced Technology Demonstration.

### 5.2 Principal Conclusions

- The basic error analysis of Newell and Yaghjian at the National Bureau of Standards (NBS) remains useful for predicting worst-case sidelobe errors arising from all significant NF measurement error sources and is summarized in equations (5, 7, 8, 9, 10). Existing error bound models conservatively estimate peak sidelobe error for sidelobes in range -20/-60 dB as shown in Figure 4. Total sidelobe error will be some weighted combination of the individual worst-case estimates. Appropriate weighted combinations depend upon the specific facility and test array. However, probable sidelobe errors are shown to be related to expected values of measurement errors (not peak values). This idea was used to develop better estimates of sidelobe errors due to probe position uncertainty in section 3.1.

• Besides positioning error, a second fundamental source of measurement error is due to multiple reflection between probe and the test array. Procedures to compensate its effect include averaging several sets of PNF data on slightly separated planes, or by using a reduced scattering cross-section probe. As shown in section 3.2, the change in measured NF phase can be determined, and used to estimate expected sidelobe error by scaling an existing peak error bound. A simulation of the scaling improvement is given in section 3.2.4.

• Finally, several new PNF probing techniques have been suggested which have the potential for minimizing FF sidelobe error. These include i) a probe designed for reduced-scattering, and ii) a probe designed to have the optimum directivity. A third new technique seeks to improve the overall NF measurement process by simplifying the data acquisition/processing burden via scanning over a highly-thinned measurement area. Navy-owned PNF test data from a moderate sidelobe array were processed in this manner and are summarized below.

### 5.3 Results

The following results are given to support the conclusions of the study.

#### 5.3.1 Multipath

Improved sidelobe error estimates are possible by using equation (18) and a scaled value of the measured peak ripple magnitude  $\epsilon^{mr}$ . Scale factors depend upon the measured multipath NF phase change. Simulation results showed that scale factors vary between .35 and 2.7 (scale factor = 1 is no scaling) for a class of tapered NF varying as  $\cos^n(\pi x/\ell_{max})$ ,  $n = 1, 2, 3$ ,  $\ell_{max}$  is aperture length. The larger scale factors increase the  $\epsilon^{mr}$  bound on the near-in sidelobes, while the smaller scale factor applies in the far-out sidelobe region. Scale factors are unique to each probe and array.

### 5.3.2 Probe Position Error

Based on the use of a compensation technique to correct the measured NF data by the known probe position errors, expected FF sidelobe error may be estimated by using equations (5,7) and probable values of the residual (i.e., compensated) random position error. Residual position errors can be assumed to occur with a truncated gaussian probability whose standard deviation is shown to depend upon the known peak position error in the scan plane (section 3.1.3).

### 5.3.3 Reduced Scattering Probe

The scattering cross-section of a typical PNF waveguide probe can be reduced by at least 50% with minor decrease in its gain by incorporating a terminal load. Reduced scattering probes will minimize the NF interference peak magnitude factor. Such probes are a needed first priority improvement in low sidelobe testing applications, since PNF theory does not presently account for NF multipath effects.

### 5.3.4 Thinned Scanning Techniques

The degree to which the PNF departs from rectangular separability dictates the degree of thinning which may be possible in the measurement plane. The results of processing thinned PNF data for a circularly symmetric Navy array antenna of moderate sidelobe design is summarized in Table 3. Thinned PNF using only 23 of 181 actually measured NF scans (12.5% of normally acquired NF data), generated 1.43 dB error at the -37.0 RMS sidelobe level and 4.0 dB peak error at the -30 dB sidelobe. For larger thinning ratios (more of the available data), even smaller pattern errors result. This error is in addition to fundamental error sources, but was investigated during this study for future utility should simple low cost PNF testing facilities be sought by the Navy.

#### 5.3.5 Optimum Probe

An optimum realizable probe for testing low sidelobe arrays is required to have physical design constraints given in section 4.3.3.2. That these constraints cannot be met with the existing class of dominant-mode waveguide probes was shown in section 4.3.3.1. An alternate class of probes was suggested to be either a single radial mode dipole operating very close to the test array ( $<1\lambda$ ), or a small probe array cluster of radial mode dipoles. Such a probe array can be designed by performing a numerical optimization study as suggested in section 4.3.3.3. The essential property of the alternate probe is to be most responsive to PNF energy propagating to the array FF sidelobes.

#### 5.4 Recommendation

The major recommendation of this DESAT phase 1 feasibility study is to experimentally confirm both the improved measurement techniques and the improved methods of estimating FF sidelobe error by conducting a DESAT phase 2 testing demonstration at the planar near field (PNF) facility of the National Bureau of Standards, using a qualified very low sidelobe array. Such a demonstration would improve the confidence of testing arbitrarily high performance array antennas by confirming the error bounding methods of this study. It would also provide the first practical evidence of the fundamental measurement accuracy associated with the PNF testing method, independent of present or future array program specific performance requirements. Finally, an original observation of this study is that an optimum probe for low sidelobe testing can not be provided by the usual dominant-mode waveguide horn now in use. A suggested alternate probe design should be implemented, evaluated, and its utility documented during the DESAT phase 2 demonstration.

6.0      REFERENCES

1.      A.C. Newell, M.L. Crawford, "Planar Near Field Measurements on High Performance Array Antennas," NBSIR 74-380, July 1974.
2.      C.E. Kirchhoff, "Antenna Pattern Measurements on the EC-135N Aircraft Using a Portable Near Field System," USAF Contract F33615-77-C-1070, Martin Marietta Corp, March 1978.
3.      A.C. Newell, et al., "Accurate Measurement of Antenna Gain and Polarization at Reduced Distances by an Extrapolation Technique," IEEE Trans Ant and Propagat. Vol. AP-21, No. 4, July 1973.
4.      Hanfling, J.D., "Planar Near Field Measurements for Aircraft Antenna Applications," 1979 Allerton Antenna Applications Symposium, University of Illinois, Sept. 1979.
5.      M.L. Crawford, "Calibration of Broadbeam Antennas Using Planar Near Field Measurements," Conference on Precision Electromagnetic Measurements, IEEE Cat No. 76CH1099-1-IM, Boulder, Colorado, July 1976.
6.      G.P. Rodrigue, et al., "An Investigation of the Accuracy of Far-Field Radiation Patterns Determined From Near-Field Measurements," (DDC ascension # AD 766776), August 1973.
7.      A.C. Newell, "Upperbound Errors in Far Field Antenna Parameters Determined from Planar Near Field Measurements - Part II - Analysis and Computer Simulation," Lecture Notes for NBS Short Course, July 7-11, 1975.
8.      A.D. Yaghjian, "Planar Near Field Measurement Techniques on High Performance Arrays - Part I: Error Analysis for Nonscanning Beam Patterns," NBS, Technical Note 667, Oct 1975 (DDC ascension # AD A014397).
9.      P.E. Wacker, "A Qualitative Survey of Near Field Analysis and Measurement," NBSIR 79-1602, National Bureau of Standards, June 1979.
10.     L.E. Corey and E.B. Joy, "Analytic Compensation for the Effects of a Warped Planar Near Field Measurement Surface on Calculated Far Field Patterns," Conference on Precision Electromagnetic Measurements, Ottawa, Canada, 1978.
11.     P.K. Agrawal, "A Method to Compensate for Probe Positioning Errors in an Antenna Near Field Test Facility," IEEE 1982 APS Symposium Proceedings, Albuquerque, N.M., May 1982.

12. J.L. Allen, "The Theory of Array Antennas," Technical Report No. 323, Massachusetts Institute of Technology, Lincoln Laboratory, July 1963.
13. D.M. Kerns, "Plane-wave Scattering-Matrix Theory of Antennas and Antenna-Antenna Interactions: Formulation and Applications," Journal of Research, NBS Vol. 80B, March 1976.
14. J.D. Kraus, Antennas (McGraw Hill Book Company), New York, 1950, p. 45.
15. L.J. Kaplan, J.D. Hanfling, "Near Field Diagnostic Study," Technical Report AFAL 77-141, Wright Patterson AFB, by Raytheon Company, Bedford Massachusetts, July 1977 (available from DDC contract No. F33615-76-C-1134).
16. L.J. Kaplan, et. al., "Rapid Measurements and Determination of Antenna Patterns Using Collapsed Near Field Data," 1977 IEEE Ant and Propagat Society International Symposium, Palo Alto, California, June 1977.
17. G.K. Huddleston "Optimum Probes for Near Field Antenna Measurements on a Plane," PhD Dissertation, Georgia Institute of Technology, August 1978, available from University Microfilms International, Ann Arbor, Michigan (#7823710).
18. P.E. Wacker, "Non-planar Near Field Measurements: Spherical Scanning," AFAL Technical Report 75-38, April 1975 (available from DDC #A012295).
19. J. R. James and L. W. Longdon, "Prediction of Arbitrary Electromagnetic Fields from Measured Data," Alta Frequenza Vol. 38, May 1969.



## APPENDIX I

### Title: Preliminary Test Plan for the Ultralow Sidelobe Near Field Measurement Study for DESAT Phase 2 Demonstration

#### 1.0 INTRODUCTION

##### 1.1 General

This appendix establishes a recommended plan of tests to be implemented at the National Bureau of Standards (NBS), Boulder, Colorado, using a qualified ultralow sidelobe array antenna and the NBS planar near field (PNF) antenna test range. This plan is the basis for conducting the DESAT phase 2 demonstration of those measurement techniques and practices developed during the phase 1 study. When completed, these phase 2 test results and their predicted tolerances, should establish the state of the measurement art for low sidelobe array antenna testing when using planar near field measurement facilities. Many of the test designs described below are based on an original set of array performance tests first undertaken by US engineers at NBS in 1973, for a moderate sidelobe array [A1].

##### 1.2 Key Test Issues

During the course of DESAT phase 1 feasibility study, the possible NF measurement error sources have been analyzed to establish the very low sidelobe FF error bound. This analysis has suggested the following key test issues to be addressed during the phase 2 demonstration.

- Scan area requirements for specified probe-to-array NF separations
- RF link dynamic range and instrumentation accuracy
- Probe/array multiple scattering effects
- Probe-position error effects
- Optimal probe pattern properties.

## 2.0 SCOPE OF TESTS

Planar NF radiation tests are herein outlined which are intended to certify newly developed or existing NF testing practices. Actual far field (FF) sidelobe levels acquired by precision NF testing, are to be compared to predicted error bounds based on analytic models reviewed during phase 1. When possible, comparisons to existing FF pattern data will also be made. However the scope of the DESAT phase 2 testing is to demonstrate the closer agreement between predicted and actual NF-measured sidelobe levels.

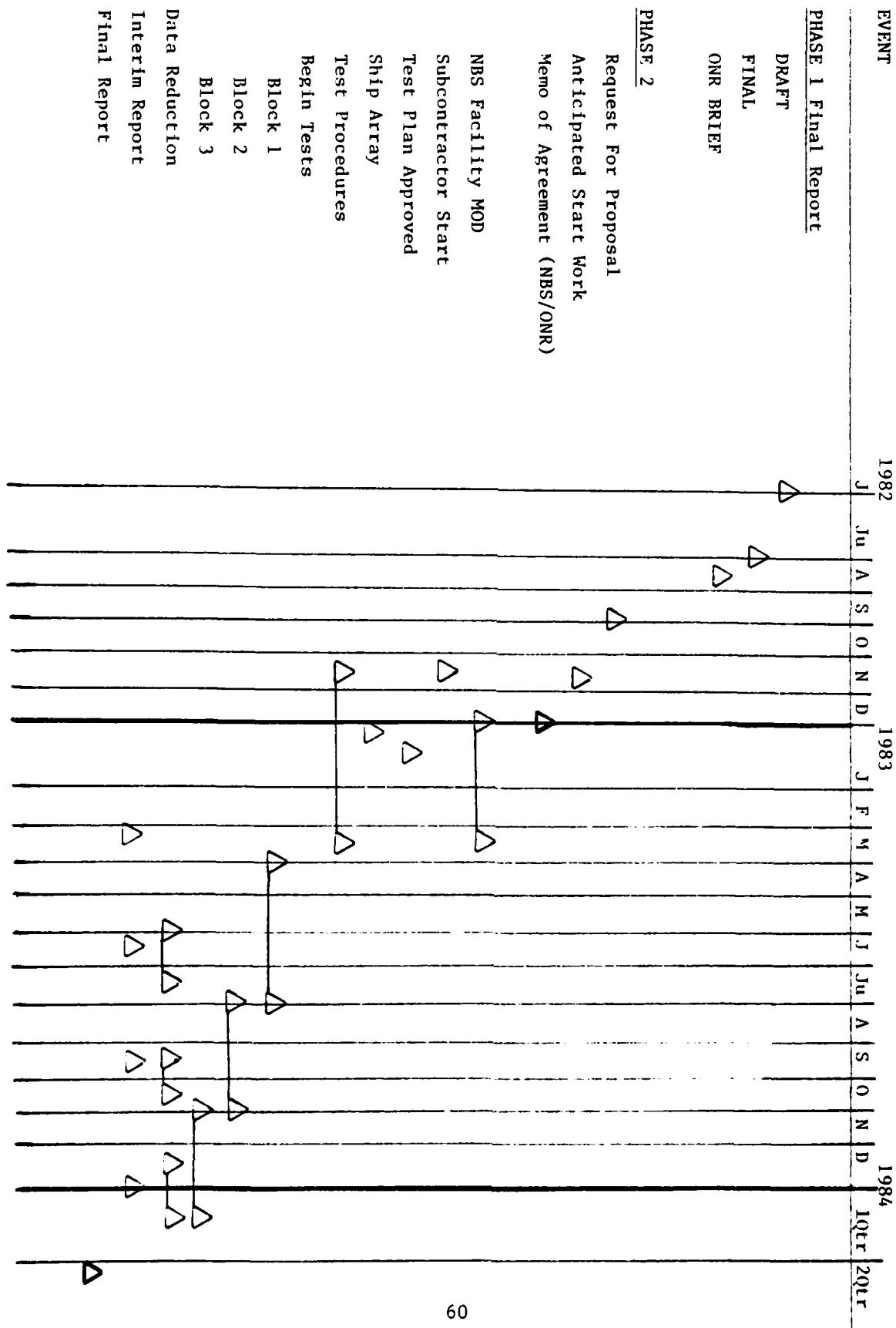
### 2.1 Limitations of Scope

Certified NF range tolerances at NBS will of course establish the ultimate accuracy of the measured array sidelobes. Methods to compensate some sources of NF measurement error will be demonstrated to show the sensitivity of low sidelobe levels to known measurement error sources. The scope of this program is limited to low sidelobe performance testing only. Other antenna properties e.g., cross pol, null depth, etc., are not of primary interest in the proposed demonstration.

### 2.2 Schedule

A schedule for the DESAT phase 2 testing is shown in Figure A1. It is provided as guidance only, and is contingent on the contracted availability of the NBS NF range (see section 4 below), and the sponsors overall DESAT work plan.

Figure A-1 Proposed DESAT Phase 2 Schedule



### 3.0 TEST ORGANIZATION

#### 3.1 Participants

The planned phase 2 test organization is shown in Figure A2. TSC will assume principal responsibility for the overall accomplishment of the phase 2 demonstration. Engineering services to be performed by TSC include:

- Test planning
- Sidelobe error estimation
- Test Results Reduction and Analysis
- Reporting
- Array Availability

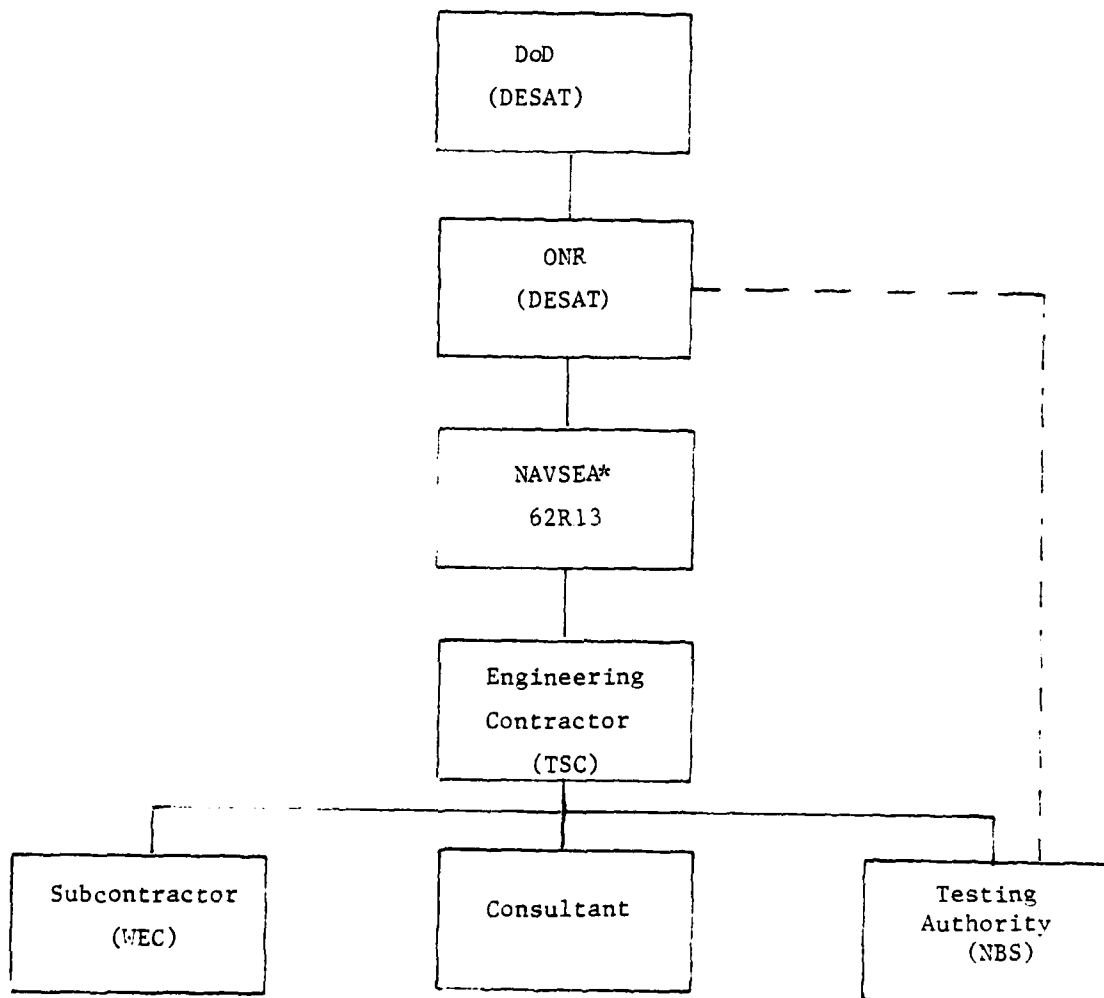
NBS Laboratories will perform all actual testing activities under direction from the TSC engineering manager, but as authorized by the technical monitor (dashed line). This flow is intended to make available the existing quality NF test range at NBS as a government-furnished facility (GFF). A suggested memorandum of agreement between ONR and NBS will be included in the DESAT phase 2 proposal.

#### 3.2 Subcontracting

TSC will provide the ultralow sidelobe array antenna as CFE (Contractor Furnished Equipment) by subcontracting for support sources from Westinghouse Electric Corporation, Defense and Space Systems Division. Either the AWACS brassboard array antenna or an experimental ultralow sidelobe S-band array will be selected as the test article, and will be fully described in the phase 2 DESAT proposal.

#### 3.3 Consulting

TSC will retain an independent consultant, Dr. Ed Joy, at Georgia Institute of Technology to provide advisory services during the conduct of the phase 2 testing. With the proposed test organization, the best available



\*Suggested

Figure A-2. DESAT Phase 2 Test Organization for  
Ultralow Sidelobe NF Measurement  
Demonstration

NF testing authorities in the US will be actively involved in the DESAT phase 2 demonstration effort as here outlined.

#### 4.0 TEST FACILITY

The NBS PNF measurement facility is a fully automated probe scanner having an active region of 4.5m x 4.5m. Peak positioning errors any where in the scan plane are about  $\pm 0.01$  cm, but are even less over smaller subregions. Figure A3 shows a photograph of the scanner with its absorber and a small aircraft fairing section mounted for test. Antennas whose maximum dimension is greater than 3.0m can be accommodated by providing a translation motion at its mounting point. Such a feature will be implemented for the DESAT phase 2 effort.

Typical NBS accuracies are 1.0dB at the -40dB relative pattern level with measurement capability to the -60dB level. Certification of these accuracies is by documented analysis. A minicomputer data acquisition system is also used to perform probe motion control. The scanning is accomplished with continuous chain and DC motor. Probe transverse position is continuously LASER monitored. RF instrumentation includes standard microwave two channel receiver and synchronized power-level RF source. This facility was used to perform the first phased array testing program in the US. Many additional test programs have since established the pre-eminence of this facility for pattern testing of directive microwave antennas. Many of the original NBS staff who took part in the first array testing program are prepared to participate in this DESAT phase 2 program.

The availability of this facility has already been coordinated with the NBS. The goal of the DESAT initiative is closely in line with existing NBS (Department of Commerce) policy to assist small business product and market development. Consequently, TSC will propose that the DESAT authority make available the NBS PNF facility as Government Furnished Facility for the conduct of the phase 2 demonstration.

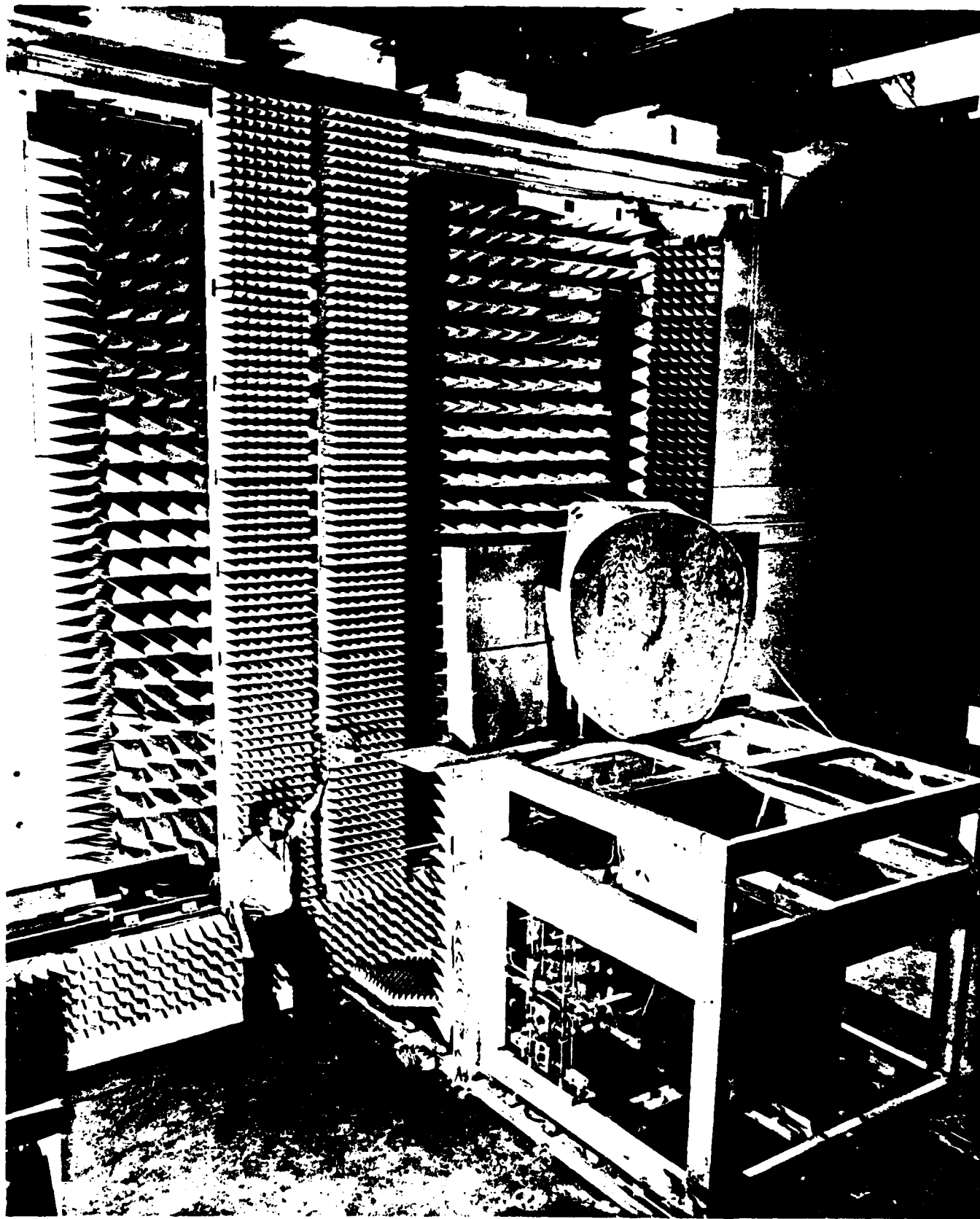


Figure A.3 NBS PNF Test Facility Proposed for Use During  
The DESAT Phase 2 Demonstration

## 5.0 TEST SUPPORT REQUIREMENTS

This section identifies the requirements for the support of the DESAT phase 2 test demonstration.

The following support categories are required.

1. Facilities
2. Instrumentation and array
3. Testing personnel

### 5.1 Facilities

#### 5.1.1 NBS Planar Scanner

This completely equipped quality NF range must be available for intermittent use during the entire phase 2 activity. A facility improvement is needed to accommodate the mounting and alignment of either of the proposed phase 2 test arrays in front of the fixed planar scanner. Approximately 3 man months of effort is needed for this modification. The array antenna is needed on site during this period.

#### 5.1.2 NF Data Processing Facility

Access to the NBS Cyber 74 computer system will be required for the preliminary NF data reduction, including raw data type editing and listing, and some data analysis programming.

#### 5.1.3 Remote Site Processing Facility

The TSC Prime 350 computer system will be used for final data reduction, including parametric variable analysis, curve plotting and statistical reporting.



## 5.2 Instrumentation and Array

The selected array must be available to NBS at start of contract plus 1 month and remain until end contract. Necessary waveguide adapters, transitions, strongback fixtures, power supplies etc., will be required. Several FF proof-of-operation RF tests on the selected array by the supplying subcontractor will be necessary prior to shipment to NBS.

## 5.3 Testing Personnel

### 5.3.1 DESAT Procuring Officer

- provide contractual authorization for the phase 2 program
- generate an Interagency Memorandum of Agreement authorizing the use of and support for the NBS NF facility as GFF.

### 5.3.2 NAVSEA Technical Monitor

- provide overall guidance to the phase 2 test team for the DESAT program manager
- coordinate the availability GFF and CFF facilities and equipment
- make periodic progress statements to the DESAT authority
- review reporting of results for technical accuracy and applicability

### 5.3.3 TSC Test Team

- prepare test designs and formulate test plan
- estimate FF sidelobe error tolerances and parametrically relate to measurement error sources
- provide test data reduction services
- participate in the conduct of key tests
- acquire and ship the candidate test array to NBS
- provide on-site assistance
- perform all detailed data reduction and analysis

5.3.4 NBS Test Team

- modify the existing NF range mounting positioner in order to accommodate the phase 2 demonstration array
- perform initial mounting and alignment tests to certify the proposed scanning strategy
- activate existing data reduction computer programs used with the original Constrained Lens Testing program
- provide a data file transfer procedure for making available edited NF data to TSC
- perform specified tests
- fabricate special probes recommended during the phase 1 study
- provide status reports

## 6.0 DATA AND MEASUREMENTS REQUIREMENTS

### 6.1 Data Sources

All NF test data will be recorded on magnetic mini disc associated with the NBS automated scanner controller. These mini-disc files will be subsequently transferred to mass storage disc files at the NBS CYBER 74 computer, and to nine track tape files for transfer to TSC. Other sources of data include

- xy recorder probe analog outputs
- manually recorded data
- support equipment calibrations

### 6.2 Performance Evaluation

Post-test evaluation reports will include header record data identifying

- time of day
- frequency
- array mode
- scan parameters
- probe separation distance

A summary of performance measures to be used as figures of merit for evaluating sidelobe level measurement accuracy, is listed in table A-1. The indicated test number are defined in paragraph 7.0 and table A-2.

Table A-1 Performance Measures for DESAT Phase 2 Testing

Performance Measures	Test No	1	2	3	4	5	6	7
1. RMS and max Change in per cent of Peak			X	X		X	X	
2. Pattern Overlays (error pattern)	X		X	X	X	X	X	X
3. Sidelobe Region RMS			X	X	X	X	X	
4. Average Level of Peak Sidelobes			X	X	X	X		
5. Sidelobe Number Distribution						X		X

(Test Number Described in Table A-2 and paragraph 7.6)

Table A-2. Test Number Description

Test Number	Description
<u>Centerline Scanning</u>	
1	Initial Alignment and Checkout
2	NF Scan Length Certification
3	NF Sample spacing Certification
<u>Planar area scanning</u>	
4	Multiple-plane sampling
5	Simulated probe-position error effects
6	Sensitivity to probe properties
7	Thinning for principal plane patterns only

## 7.0 TEST DESIGN

### 7.1 Initial Check Out and Pre-Test Preparation

This section outlines those tasks necessary to insure that the test array is adequately operating, mounted, and aligned with respect to the NF scanner.

#### 7.1.1 Mounting Certification

The DESAT test array will be mounted on the modified array positioner and laterally translated right and left from a reference location. Center-line NF amplitude and phase data shall be acquired to demonstrate the adequacy of the proposed "scan-length-merging" sampling strategy.

#### 7.1.2 Pre-Test Preparation

All normal instrumentation calibration, initial multipath estimates, probe position reference tests, etc., shall be performed prior to the conduct of performance tests below.

#### 7.1.3 Probe Calibration Tests

Existing or newly developed probes for this test program shall be independently calibrated by FF pattern testing for the purpose of DESAT array probe correction data processing.

### 7.2 Performance Testing

This section describes those tests needed to verify those predictions of sidelobe accuracy made during DESAT phase 1 feasibility study, and to resolve the key test issues in section 1.1. The descriptions given refer to the numbered tests in tables A-1 and A-2.

#### 7.2.1 Test 2 - Scan Length Certification

Technical Objective: This test will certify the predicted minimum scan length criterion by measuring the DESAT array sidelobe sensitivity to decreasing probe scan length, and by comparing these results to known scan length requirements and to previous results for moderate sidelobe arrays. Scan length restrictions which will produce sidelobe error of specified magnitude will be established.

#### 7.2.2 Test 3 - Sample Spacing Certification

Technical Objective: This test will certify the predicted sidelobe sensitivity due to possible values of measurement sample spacing in the scan dimension, and will compare these test results to known sidelobe sensitivities for moderate sidelobe arrays.

#### 7.2.3 Test 4 - Multiple Plane Sampling

Technical Objective: This test will acquire the facility-unique performance data necessary to predict the worst-case and probable sidelobe error due to NF multipath. Additionally those improved probing techniques, developed during phase 1 to compensate multipath measurement error, will be exercised.

#### 7.2.4 Test 5 - Simulated Probe Position Error Effects

Technical Objective: This test will purposely corrupt measured DESAT NF data (assumed error free) by adding synthetic amplitude and phase error, in accordance with probe position error models studied during phase 1. The sensitivity of the transformed FF sidelobes to those artificial errors will confirm the predicted worst case positioning error magnitudes and form. An actual position error correction will be performed on the artificially corrupted data. The residual random error should generate sidelobe errors as predicted in Section 3.1 of the phase 1 study.

7.2.5 Test 6 - Sensitivity to Probe Properties

Technical Objective: This test will quantify the dependence of sidelobe errors on probe/array scattering and on the newly developed concept of an "optimum" probe for low sidelobe testing developed during the phase 1 study.

7.2.6 Test 7 - Principal Plan NF Testing

Technical Objective: This test will quantify the residual sidelobe error which results from thinning two dimensional NF data in the dimension orthogonal to the desired single pattern transform plane. This test will confirm the thinned-sampling strategy development during phase 1 when applied to low sidelobe arrays.



REFERENCES (For Appendix I)

1. "Planar Near Field Measurements on High Performance Array Antennas," NBSIR 74-380, July 1974 by A.C. Newell and M.L. Crawford, as also referenced in the test as Reference #1.

DATE  
FILMED  
8

